DESIGN, ANALYSIS, TESTING AND DEVELOPMENT OF A THERMOACOUSTIC SYSTEM FOR REFRIGERATION APPLICATIONS

Masoud Akhavanbazaz

A Thesis

in

The Department

Of

Mechanical and Industrial Engineering

Presented in Partial Fulfillment of the Requirements

for the Degree of Master of Applied Science at

Concordia University

Montreal, Quebec, Canada

September 2004

Your file Votre référence
ISBN: 0-612-94721-1
Our file Notre référence
ISBN: 0-612-94721-1

ABSTRACT

Design, Analysis, Testing and Development of a Thermoacoustic System for Refrigerator Applications

Masoud Akhavanbazaz

Thermoacoustic deals with the conversion of heat energy to sound energy or vice versa. Thermoacoustic cooling devices use the thermoacoustic principle to move heat using sound. They consist of a standing wave tube in which a stack of fractional wavelength creates a temperature gradient across the stack, facilitating heat flow. These devices are simple in design and have no harmful effects on the environment. However, their efficiencies are lower than the conventional vapor-compression refrigeration systems. In this study, the design, and development of a thermoacoustic system for refrigeration application was considered. This study comprised two parts. In the first part, different components of the thermoacoustic refrigerator were designed based on the numerical analysis. In the second parts, the refrigerator was fabricated based on the numerical design. The performance of the device was then tested and analyzed.

The numerical study has shown that the stack length and the position of the stack in the resonator have a significant impact on the overall performance of the thermoacoustic device. Air at standard temperature and pressure is employed as the working gas. The acoustic power source was a 15 W speaker operating at a frequency of 450 Hz. Based on a numerical study, the stack length was set equal to 3 cm with its center located at a distance of 5 cm from the driver-end of a 38.5 cm long resonator tube. The temperature difference between the two ends of the stack was set equal to 25 K.

A thermoacoustic refrigerator was developed based on the designed parameters. Preliminary experimental results have shown that a temperature difference of as high as 23 K was established across the stack. In order to exploit the thermoacoustic effect for heat pumping; heat exchangers were attached at both ends of stack. Water at ambient temperature was chosen as the working fluid for the heat exchangers to facilitate heat transfer to or from the stack. A pump was used to circulate water through both heat exchangers. Experimental results have shown that water temperature difference of 3 K for cold heat exchanger and 7.5 K for hot heat exchanger were established. The maximum coefficient of performance (COP) of this device was 1.5. Further research and development is needed in order to explore the full potential of the device in refrigeration applications.

ACKNOWLEDGMENTS

I wish to express my heartfelt and profound gratitude to my supervisors Dr. Kamran Siddiqui and Dr. Rama B. Bhat for their invaluable guidance, assistance and inspiration throughout the span of this work and for their helpful financial support.

I would also like to express my deep appreciation to Mr. John Elliott, Mr. Danny Juras, Mr. Brian Cooper and Mr. Gilles Huard for their nice cooperation.

CONTENTS

List of Figures

List of Tables

Nomenclature

Lower case

a	sound velocity	[m/s]
f	frequency	[Hz]
f_k	thermal Rott function	
f_v	viscous Rott function	
h	specific enthalpy	[J/kg]
I	electrical current	[A]
i	imaginary unit	
k	wave number	[m^{-1}]
l	plate half-thickness	[m]
m	mass	[kg]
p	pressure	[Pa]
r	resonator radius	[m]
s	specific entropy	[J/kgK]
t	time	[s]
u	x-component of velocity	[m/s]
v	y-component of velocity	[m/s]
w	z-component of velocity	[m/s]
x	position along sound propagation	[m]
x_s	position of the stack	[m]
y	position perpendicular to sound propagation	[m]
y_0	plate half-gap	[m]

Upper case

A	area	[m^2]
B	blockage ratio	
C_p	isobaric specific heat	[J/kgK]
C_v	isochoric specific heat	[J/kgK]
C_s	specific heat of the stack material	[J/kgK]
D	drive ratio, or diameter	[m]
E	total power	[W]
F	force	[N]
H	enthalpy	[J]
K	thermal conductivity	[W/Km]
K	temperature	[K]
Im	imaginary part of	
Re	real part of	
L	length, sound pressure level	[m]
M	molecular weight	[kg/kmol]
P	power	[W]
Q	heat flux	[W]
R	the universal gas constant	[J/mol.K]
S	entropy	[J/K]

T	temperature	[K] or [^{0}C]
U	volumetric velocity	[m^3/s]
V	voltage [V], or volume	[m^3]
W	acoustic power	[W]

Lower case Greek

β	thermal expansion coefficient	[K^{-1}]
γ	ratio of isobaric to isochoric specific heats	
δ	penetration depth	[m^{-1}]
ε	maximum energy of attraction	
ε_s	stack heat capacity ratio	
η	efficiency	
κ	thermal diffusivity	[m^2/s]
λ	wave length	[m]
μ	dynamic viscosity	[Pa.s]
ν	kinematic viscosity	[m^2/s]
ξ	second viscosity	[Pa.s]
ρ	density	[kg/m^3]
σ	Prandtl number	
σ'	viscous stress tensor	[N/m^2]
θ	phase angle difference	[rad]
ω	angular frequency	[rad/s]

Upper case Greek

Γ	normalized temperature gradient	
Π	perimeter	[m]

Sub- and superscripts

ac	acoustical
C	Carnot, or cold
CHX	cold heat exchanger
crit	critical
d	driver
e	electrical
g	gas
H	hot
h	hydraulic
HHX	hot heat exchanger
hp	heat pump
k	thermal
m	mean, or mechanical
res	resonator
s	standing, or solid

st	stack
x	along sound-propagation direction
tot	total
ν	viscous
0	amplitude
1	first order
2	second order

Chapter 1

Introduction and Literature Review

Recent developments in the field of thermoacoustics promise to revolutionize the way that many machines currently operate. By manipulating the temperature-changes along the acoustic longitudinal waves, a machine can be created that can replace current refrigeration and air conditioning devices. These machines can be integrated into refrigerators, home generators, hot water heaters, or space heaters and coolers. The thermoacoustic devices contain no adverse chemicals or environmentally unsafe elements that are characteristics of the current refrigeration systems.

Thermoacoustics deals with the conversion of heat energy to sound energy and vice versa. There are two types of thermoacoustic devices: thermoacoustic engine (or prime mover) and thermoacoustic refrigerator. In a thermoacoustic engine, heat is converted into sound energy and this energy is available for the useful work. In this device, heat flows from a source at higher temperature to a sink at lower temperature. In a thermoacoustic refrigerator, the reverse of the above process occurs, i.e., it utilizes work (in the form of acoustic power) to absorb heat from a low temperature medium and reject it to a high temperature medium. The efficiency of the thermoacoustic devices is currently lower than that of their conventional counterparts, which needs to be improved to make them competitive. In addition, other considerations for a

competitive thermoacoustic device are low cost, high reliability, safety, compactness, and ease of mass production.

1.1 Thermoacoustic Phenomenon

Acoustic waves experience displacement oscillations, and temperature oscillations in association with the pressure variations. In order to produce thermoacoustic effect, these oscillations in a gas should occur close to a solid surface, so that heat can be transferred to or from the surface. A stack of closely spaced parallel plates is placed inside the thermoacoustic device in order to provide such a solid surface. The thermoacoustic phenomenon occurs by the interaction of the gas particles and the stack plate. When large temperature gradients are created across the stack, sound waves are generated i.e. work is produced in the form of acoustic power (forming a thermoacoustic engine). In the reverse case, the acoustic work is used in order to create temperature gradients across the stack, which is used to transfer heat from a low temperature medium to a high temperature medium (as the case of a thermoacoustic refrigerator).

A thermoacoustic refrigerator consists of a tube filled with a gas. This tube is closed at one end and an oscillating device (e.g. a piston or loud speaker) is placed at the other end to create an acoustic standing wave inside the tube. To understand the thermoacoustic cycle in a thermoacoustic refrigerator, consider a parcel of gas inside the tube with a piston attached to one end of the tube (as shown in Fig. 1.1). The gas parcel oscillates due to the oscillations of the piston. Consider four stages of the piston oscillations, which comprises a thermodynamic cycle consisting of four processes. Two

of these processes are reversible adiabatic (1 and 3) and the other two are isobaric (2 and 4), as shown in Fig. 1.1.

If the temperature gradient at the wall is very small or zero, this process is called heat pumping (or refrigeration). During the first process, the piston moves toward the closed end and compresses the parcel of the gas, and hence the gas parcel warms up. During the second process, heat flows irreversibly from the parcel to the wall, because the temperature of the gas is higher than that of the wall due to compression. During the third step, the piston moves back (i.e. towards the right side), and the gas parcel expands and cools.

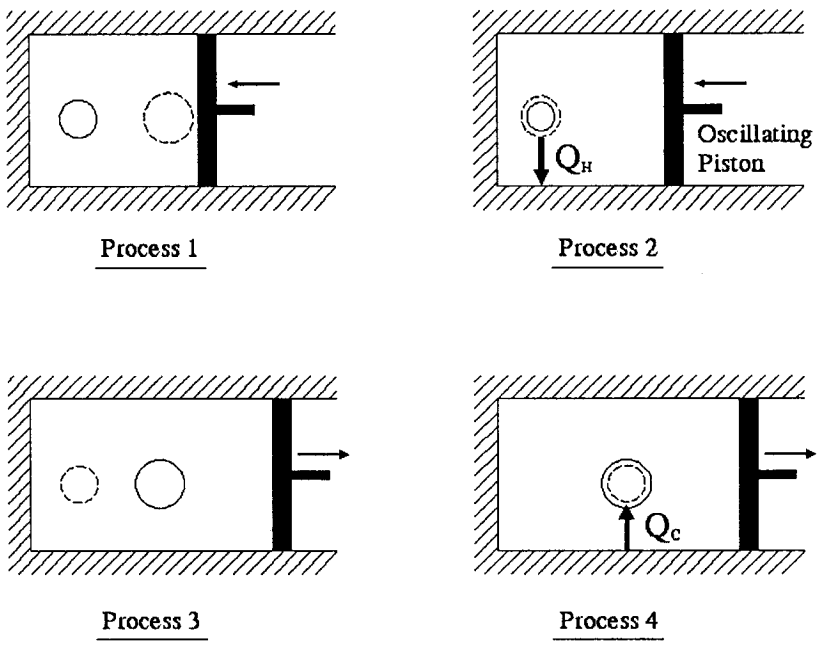

Figure 1.1: Thermoacoustic Cycle.
Solid circle shows the parcel state at the beginning of process and the dashed circle shows the parcel state at the end of process.

At the end of the third process, the temperature of the gas parcel is less than the wall temperature. During the fourth and last process, heat flows irreversibly from the wall to the gas parcel. At the end of this process, the gas parcel returns to its initial state and the thermoacoustic cycle is completed. Thus, during the complete cycle, a net amount of heat is transferred from one end of the tube to the other by the gas parcel under the influence of externally generated oscillations. If this cycle continues, one side of the tube warms up and the other side cools down creating a temperature gradient. The tube mentioned should not be conducting heat in order to maintain the temperature gradient. In conventional systems, pistons are used to compress and move the gas, but in thermoacoustic devices, compression and displacement occur by the acoustic wave, and the time phasing is necessary to have irreversible heat transfer in steps 2 and 4 because of the time lag between the temperature and the particle motion.

It is important to know that all the gas parcel inside the tube do not contribute equally in the thermoacoustic effect. The parcels of gas that are far away from the wall do not have thermal contact with wall. The parcels that are too close to the wall have a good thermal contact but also have significant viscous effects. An optimal distance of the gas parcel for the best performance is the one where the viscous effects are minimal and the thermal contact with the wall is strong enough for the heat exchange. The optimal distance is related to the thermal and viscous penetration depths that will be discussed in detail in the next chapter.

1.2 Literature Review

The idea of using sound waves for cooling gained interest in the 1960s. Even though the physical explanation of this refrigeration technique is simple, analysis of the phenomenon and the equations that describe it are not simple. The discovery of the thermoacoustic phenomenon goes back to more than a century ago; however, the significant work in this area was started about two decades ago at the Los Alamos National Laboratory. They have developed different types of thermoacoustic refrigerators and heat engines [1]. A few other research groups are also working in this area. However, the development of such devices is still at preliminary stages. Garret et al. [2] developed a new spacecraft cryocooler, which uses resonant high-amplitude sound waves in inert gases to pump heat, which was used in the space shuttle Discovery. Tijani et al. [3] achieved temperature as low as -65 ^{o}C in their thermoacoustic device. They used it to study the effect of some important thermoacoustic parameters, such as the Prandtl number by using binary gas mixture. Bailliet et al. [4] measured the acoustic power flow in the resonator of a thermoacoustic refrigerator by using Laser Doppler Anemometry (L.D.A) together with microphone acoustic pressure measurement. They found good agreement between the experimental and theoretical results. Jin et al. [5] studied thermoacoustic phenomenon in a pulse tube refrigerator. They used a thermoacoustic prime mover to create an acoustic wave to drive the refrigerator. They studied the characteristics of the thermoacoustic prime mover and the effect of working fluid i.e. helium and different percentage of helium- argon mixture, on the thermoacoustic refrigerator. They achieved a cryogenic temperature of 120 K in their experiments. Symko et al. [6] used thermoacoustic refrigerator and prime mover to remove heat from

an electronic circuit. They drove the thermoacoustic devices at frequencies between 4-24 kHz and investigated the performance of the devices. Jebali et al. [7] analyzed experimentally the performance of a thermoacoustic refrigerator subjected to variable loading and compared the experimental data with the computed data. In their experiments, the hot heat exchanger was maintained at ambient temperature and the temperature of the cold heat exchanger was varied to achieve temperature differences of 0.5 and 10 K along the stack. They measured and calculated cooling load for these temperature differences while varying the driving frequency between 30 and 65 Hz. Sakamoto et al. [8] conducted experiments on a thermoacoustic cooler consisting of acoustic loop-tube with two stacks inside. Stack 1 was employed as a prime mover and stack 2 as a heat pump. They used the mixture of air and helium gas at the atmospheric pressure as the working fluid. They observed a temperature drop of approximately 16 ^{o}C. They also found that the self-sustained sound had higher harmonics which lowered the efficiency of the system. Tijani et al. [9] described an analytical model of the interaction between a sound wave and a solid surface. They found that the thermal-relaxation dissipation at the gas is minimal whenever the temperature oscillations in the wall follow the temperature oscillations in the gas. They concluded that a tube material with the smallest possible combination $K\rho C_s$ (where K, ρ, C_s are thermal conductivity, density, and specific heat of stack, respectively) and a gas with the largest possible combination $K_g\rho_g C_p$ could minimize the thermal-relaxation losses. Huelsz et al. [10] found expressions for the phase difference, α, between the temperature and pressure waves by using a single-plate, linear theory for the thermoacoustic phenomenon at ideal conditions (zero Prandtl number and infinite heat capacity for the plate). Wetzel and Herman [11, 12] used

a combination of holographic interferometry and high-speed cinematography to visualize and quantify the temperature fields in the vicinity of stack plate located between pressure and velocity nodes of an acoustic standing wave. They found that the heat is transferred either from the working fluid to the plate or vice versa. They measured the heat fluxes transferred from the colder fluid to the hot stack plate at the edge of a single stack plate and they investigated the difference between heat transfer in a steady forced convection and oscillatory flow. Ishakawa et al. [13] obtained a relationship between the size of the hot and cold exchangers and entropy generation rates in a thermoacoustic device and the temperature differences along the regenerator stack and their location in the resonator. They found that the heat transfer effect is more important than the viscous effect in the quick decrease of the entropy generation. In their study, they found that the size of the heat exchanger at the hot side of the regenerator stack should be smaller than that at the cold side. Ishikawa and David [14] numerically investigated the influence of the stack plate length when the plate spacing is greater than the thermal penetration depth. They observed that there was a heat-pumping effect on the long and short plates compared with the particle displacement length of the acoustic standing wave. Further, the energy dissipation close to the plates increases quadratically with the particle displacement and they found no heat transfer when the plate spacing was equal to the thermal penetration depth. Waxler [15] studied the acoustic disturbance theoretically. He solved a complete set of time-averaged second-order equations of fluid dynamics of a viscous, thermally conducting fluid between closely spaced parallel plates, when the derivative of the temperature in the absence of the acoustic disturbance with respect to x (the direction of plate length) is not equal to zero. Raspect et al. [16] used the finite difference method to

solve the equations of thermoacoustic refrigerator, thermoacoustic engine and Stirling regimes. They assumed short stack and linear temperature gradient across the stack. They solved the equations for both standing and traveling wave and compared the results with the measured values. Tijani et al. [17] explained in detail the designing criteria for thermoacoustic refrigerator in order to achieve an optimal system. They used the linear thermoacoustic theory to describe the design criteria. They used dimensionless independent variables to decrease the number of parameters and to simplify the equations. They established a method to obtain the optimum design of the different parts of the thermoacoustic refrigerator. Benson et al. [18] simulated a thermoacoustic device and numerically investigated the unsteady flow and the temperature field in the vicinity of an idealized thermoacoustic refrigerator. The numerical model simulates the unsteady mass, momentum, and energy equations in the thin-plate, and low Mach-number limits. They also analyzed the variations of the thermal performance of the device against the heat exchanger length and position. Biwa et al. [19] measured the phase angle dependence of the cooling power of a Gifford-McMahon refrigerator for the regenerator spherical particles with different diameters. Reid et al. [20] used a thermoacoustic refrigerator with a steady flow parallel to the thermoacoustic oscillations passing through the stack, in order to compare numerical studies with the experimental results for the stack temperature profile and the cooling power. Herman and Wetzel [21] presented a methodology for estimating and designing the thermoacoustic refrigerator components to obtain an optimized device. Piccolo et al. [22] presented a methodology to investigate the origin of the deviations of the predictions of the linear theory and compared them with

the measured performances of a thermoacoustic device. Tijani et al. [23] studied the effect of plate spacing and plate geometry in the stack on the performance of the device.

Thermoacoustic refrigerator is a device that operates efficiently by using sound waves, environmentally friendly and non-flammable gases, and is suitable for handling residential refrigeration needs. The thermoacoustic refrigerator has only one moving part (acoustic driver that generates the standing wave), and is relatively simple and inexpensive to construct and operate. Thermoacoustic refrigerators tend to be compact and lightweight, and contain no harmful refrigerants, which make them environmentally friendly. This aspect will make it a very appealing option in the future.

The Ozone-depleting Substances Regulations, were made under the Canadian Environmental Protection Act (CEPA) in December 1998. It is in line with The Montreal Protocol, which is an international agreement, signed by 165 countries to control the production and exchange of certain ozone-depleting substances [24]. The Regulations control the import, export, transit shipment, manufacture, use, sale and offer for sale of any HCFCs or products that contain or are intended to contain HCFCs. Under these Regulations, the manufacturing and import of many products that contain HCFCs have been prohibited since July 1, 1999, and the offers for sale and sale of many products that contain HCFCs have been restricted since January 1, 2000 [24]. Some of important advantages of a system based on thermoacoustic principle are:

- Environmental Friendliness:

No environmentally hazardous refrigerants are needed and only inert gases that are environmentally safe and suitable are used. The international restriction on the use of

CFC (chlorofluorocarbon) and skepticism over the replacements of CFC, gives thermoacoustic devices a considerable advantage over traditional refrigerators. The gases used in these devices are (e.g. helium, xenon, air) harmless to the ozone and have no greenhouse effect. It is expected that in the near future, regulations will be tougher on the greenhouse gases. The awareness about the destructive effects of CFC on the ozone depletion and the banning of the CFC's production, lead the researchers to find an alternative solution to this problem. In this scenario, thermoacoustic refrigerator could be the most suitable candidate to replace the conventional vapor-compression refrigeration systems. In addition, the thermoacoustic cycle also lends itself well to a more efficient proportional control rather than the primitive binary control that conventional refrigerators currently employ. All of these reasons make thermoacoustic refrigerator potentially attractive for widespread use.

➢ Economy:

The device can be produced and operated cheaper than the traditional vapor compression refrigerator due to the following reasons:

- Mechanical simplicity and very few number of components.
- No need for lubricants since there is only one moving part, which is the acoustic driver.
- No expensive components.
- Use of cheap and readily available gases.
- Power saving by proportional control: output of the device can be turned up or down gradually in contrast to vapor compression refrigerator's on/off control.
- Lower life-cycle cost.

However, the thermoacoustic refrigerators are currently less efficient than the conventional refrigerators, and significant efforts are needed to improve their efficiency [24].

1.3 Objectives

Even though thermoacoustic devices have been known for 30 years, there are several aspects which are not well understood. The gas behavior inside the resonator tube, its interaction with the solid surface (e.g. stack plate, Heat exchanger) and its effect on the heat transfer are not known. Better understanding of the fundamental process is necessary to improve the design of these devices. The long-term objective of this research is to develop efficient thermoacoustic devices. As a first step, which is the objective of this thesis project; analyzing, designing, and fabricating a simple and fundamental prototype thermoacoustic refrigerator and test it to study the performance. As far as we know, the work presented in this thesis is the first research on thermoacoustic devices done at any Canadian University.

1.4 Scope of the Thesis

This thesis focuses on the design, fabrication, testing, and analysis of a thermoacoustic refrigerator. In chapter 2 the basic thermodynamic and acoustic principles applied in thermoacoustic refrigerator will be reviewed. Chapter 3 is concerned with the theoretical design of the prototype. Fabrication and experimental setup are described in chapter 4 along with the experimental techniques for the measurements subsequently, in chapter 5, the experimental results obtained in this work will be presented and discussed, and finally the conclusion and suggestions for future work will be discussed in chapter 6.

Chapter 2

Thermodynamic and Acoustic Considerations in a Thermoacoustic Refrigerator

This chapter presents basic thermodynamic and acoustic principles and discusses their contribution to the thermoacoustic phenomenon. The general working principles of the refrigerator and heat pump, and the thermodynamic behavior of the gas oscillations in the stack channel will also be discussed.

2.1 Basic refrigeration theory

The refrigerator is a device that transfers heat from a low-temperature medium to a higher temperature using external work input. The working fluid used in the refrigerator is called the refrigerant. The refrigeration process is based on the first and second law of thermodynamics, and its operation is based on one of the thermodynamic refrigeration cycles. The most commonly used refrigeration cycle is the vapor-compression type.

2.1.1 Vapor-Compression Refrigeration Cycle

The vapor-compression refrigeration cycle is the most widely used cycle for refrigerators, air-conditioning systems, and heat pumps. It consists of four thermodynamic processes, and involves four main components: compressor, condenser,

expansion valve, and evaporator, as shown in Fig. 2.1. The refrigerant enters the compressor as a saturated vapor at a very low temperature and pressure (state 1). The compression process takes place inside the compressor. Both the temperature and pressure of the refrigerant increase as a result, and the refrigerant becomes superheated vapor at the exit of the compressor (state 2). At this state, the temperature of the refrigerant is greater than the temperature of the high-temperature medium. The refrigerant then enters the condenser. The heat transfer process takes place in the condenser at a constant pressure, where heat is transferred from the refrigerant to the high-temperature medium. As a result, there is a small decrease in the temperature of the refrigerant as it exits the condenser (state 3). The refrigerant then enters the expansion valve in which the temperature and pressure of the refrigerant drop significantly due to the sudden expansion. At the end of the expansion process, the temperature of the refrigerant becomes lower than that of the low-temperature medium (state 4). The refrigerant then enters the evaporator where heat is transferred from the low-temperature medium to the refrigerant at constant pressure, resulting in a small increase in the temperature of the refrigerant. At the exit of the evaporator, the refrigerant reaches the state 1 again. The refrigeration cycle is then repeated when the refrigerant enters the compressor [25]. The four processes of ideal vapor-compression refrigeration cycle are plotted on a T-S diagram in Fig. 2.1(b).

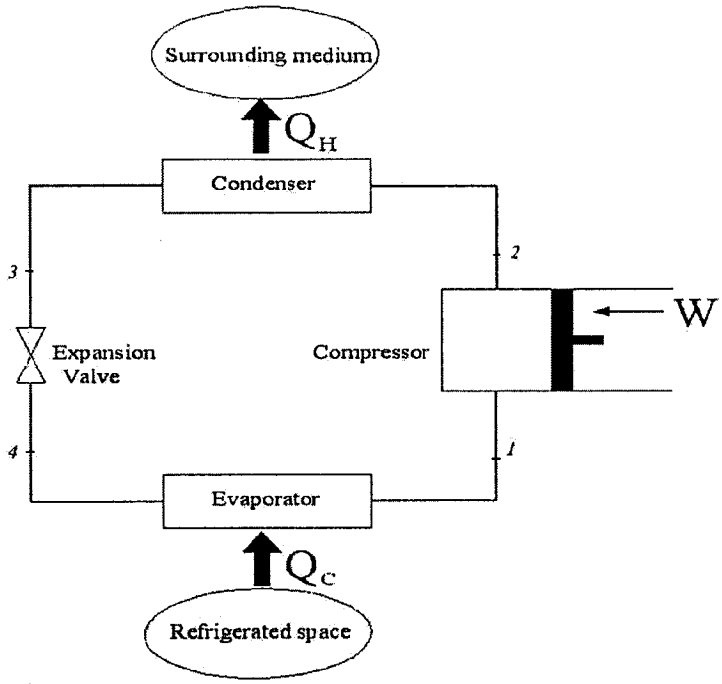

Figure 2.1(a): Basic component of a refrigeration system working on the vapor-compression refrigeration cycle.

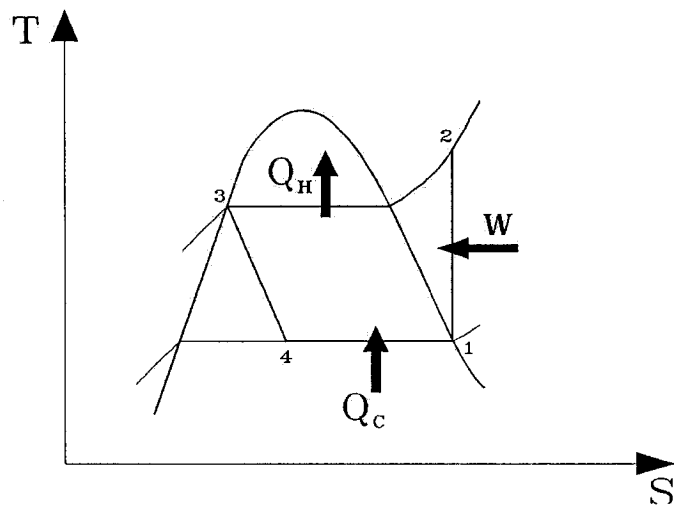

Figure 2.1(b): T-S diagram for the ideal vapor-compression refrigeration cycle.
1-2 Isentropic compression in a compressor.
2-3 Constant pressure heat rejection in a condenser.
3-4 Throttling in an expansion device.
4-1 Constant pressure heat absorption in an evaporator.

2.1.2 Coefficient of Performance (COP) of the Refrigerator

Let T_H and T_C be the temperatures of high-, and low-temperature mediums, respectively, as shown in Fig. 2.2. Also let Q_C be the amount of heat extracted by the refrigerator from the low-temperature medium and Q_H be the amount of heat delivered by the refrigerator to the high-temperature medium. If W is the work input to the refrigerator in the form of the compressor work, then according to the first law of thermodynamics .

$$Q_H = Q_C + W \tag{2.1}$$

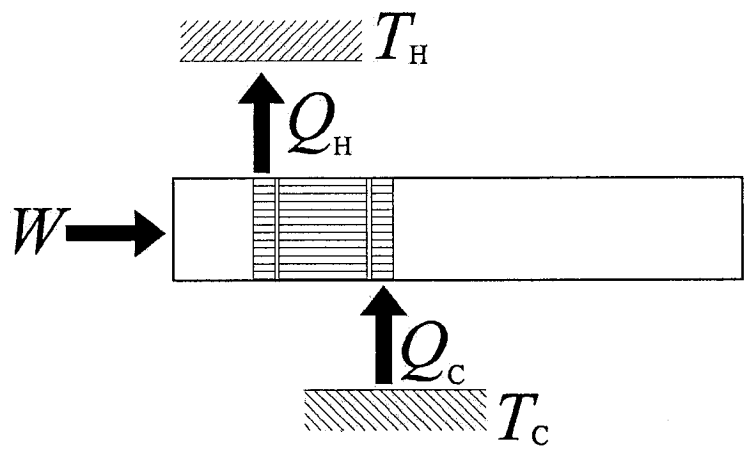

Figure 2.2: A refrigerator, showing the energy flow process.

That is, the amount of energy transferred to the high-temperature medium must be equal to the sum of the energy transferred from the low-temperature medium and the work input to the refrigerator [25]. Similarly, according to the second law of thermodynamics,

$$\frac{Q_H}{T_H} = \frac{Q_C}{T_C} + (S)_{gen} \tag{2.2}$$

where S is the entropy generation due to the irreversibility [25].

The performance of a refrigerator is measured in terms of the Coefficient of Performance (*COP*). It is defined as the ratio of the desired heat transfer to the work input. The main objective of the refrigerator is to maintain the temperature of the low-temperature medium by constantly removing the heat that leaks into the cold space from the surroundings at a higher temperature. Thus, the desired heat transfer for the refrigerator is Q_C. Hence the *COP* of the refrigerator is defined as

$$COP = \frac{\text{Re}\,moved\ heat}{Work\ done} = \frac{Q_C}{W} \tag{2.3}$$

Using Eq. (2.1), the above equation becomes,

$$COP = \frac{Q_C}{Q_H - Q_C} \tag{2.4}$$

Since for all real processes, $(S)_{gen} \geq 0$,

$$\frac{Q_H}{T_H} \geq \frac{Q_C}{T_C} \tag{2.5}$$

and

$$\frac{Q_H}{T_H} - \frac{Q_C}{T_C} \geq 0 \tag{2.6}$$

Combining the above equations, we get,

$$COP = \frac{Q_C}{Q_H - Q_C} \leq \frac{T_C}{T_H - T_C} \tag{2.7}$$

but,

$$COP_C = \frac{T_C}{T_H - T_C} \tag{2.8}$$

where COP_C is the coefficient of performance of the ideal refrigerator that works on the Carnot cycle (also known as Carnot refrigerator). Eq. (2.7) indicates that the *COP* of a refrigerator must be less than or equal to that of the Carnot refrigerator [25].

Heat pumps are devices that perform the same work as refrigerator. The main difference between the heat pump and refrigerator is the desired heat transfer. For the heat pump, the main objective is to maintain the high-temperature medium at the required temperature and this temperature is maintained by extracting heat from the low-temperature medium and delivering it to the high-temperature medium. Thus, the *COP* of the heat pump is different from the *COP* of the refrigerator [25,]. The *COP* of the heat pump is defined as,

$$COP_{hp} = \frac{Heat\ Supplied}{Work\ done} = \frac{Q_H}{W} \tag{2.9}$$

2.2 Acoustical theory

The understanding of acoustic wave dynamics, i.e. the pressure and velocity fields created by an acoustic wave, is necessary to understand the working of a thermoacoustic device. The acoustical theory deals with the study of the longitudinal acoustic waves. The longitudinal acoustic waves are generated as a result of the compression, and expansion

of the gas medium. The compression of a gas corresponds to the crest of a sine wave, and the expansion corresponds to the troughs of a sine wave. An example of how these two relate to each other is shown in Fig. 2.3. In a longitudinal wave, the particle displacement is parallel to the direction of wave propagation i.e., they simply oscillate back and forth about their respective equilibrium positions. The compression and expansion of a longitudinal wave result in the variation of pressure along its longitudinal axis of oscillation. A longitudinal wave requires a material medium such as air or water to travel. That is, they cannot be generated and/or transmitted in a vacuum. All sound (acoustic) waves are longitudinal waves and therefore, hold all the properties of the longitudinal waves discussed above. Three characteristics of the acoustic wave are necessary for the understanding of the thermoacoustic process. These properties are amplitude, frequency and wavelength.

The displacement of a wave from its equilibrium position is called the wave amplitude. It is also a measure of the wave energy. Larger the amplitude, higher will be the wave energy or intensity. Thus, the energy of an acoustic wave can be estimated by measuring its amplitude. The energy or intensity of an acoustic wave is measured in terms of decibel. If the given acoustic wave is comprised of the superposition of different sine waves, then the amplitude and hence the energy of the given wave can be estimated by integrating the energy in all the frequency components of the given wave. The time period of a wave is the time required for the complete passage of a wave at a given point. The fundamental wave frequency is the inverse of the time period. In other words, it is the number of waves that pass a given point in a unit time. It is typically measured in Hertz (Hz), that is, the number of waves that pass a given point in one second.

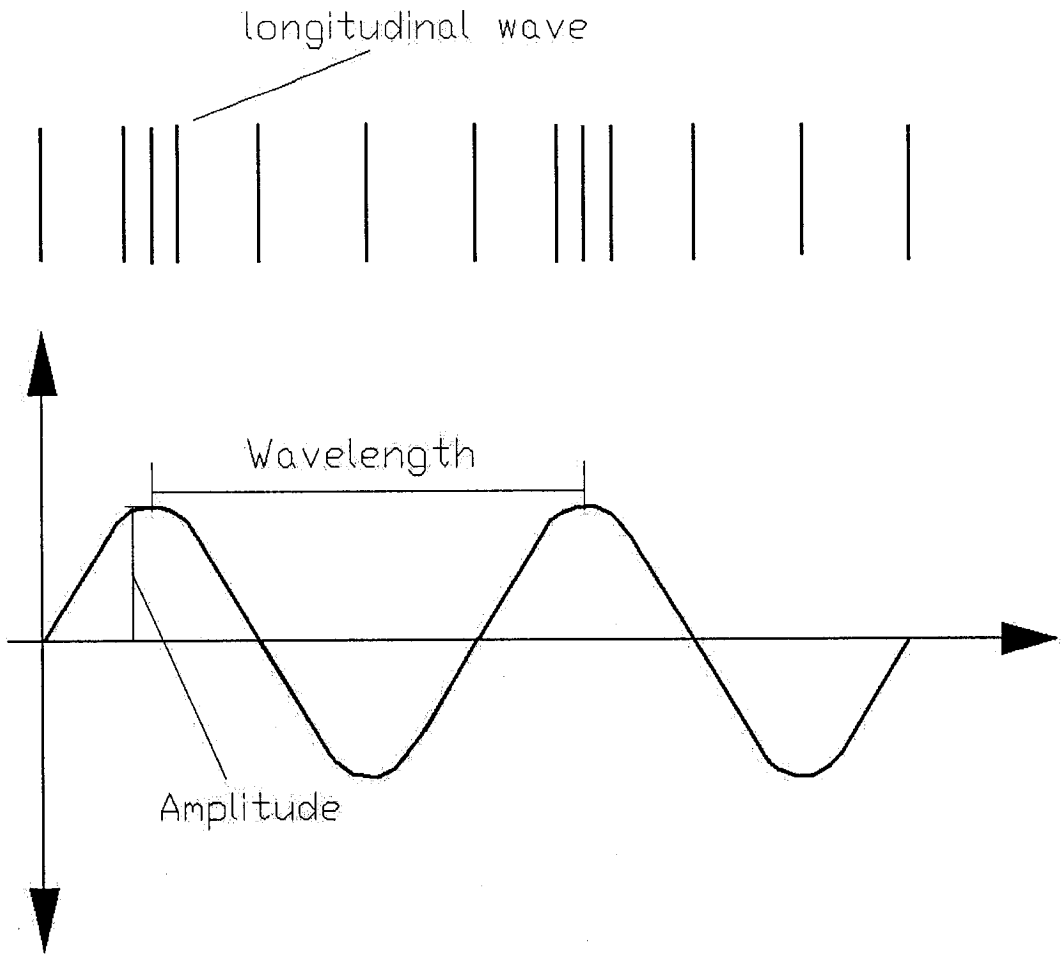

Figure 2.3. Comparison of a longitudinal acoustic wave with a sine wave.

In acoustics, it is also a measure of the sound pitch. Higher the frequency, higher will be the pitch.

The wavelength is defined as the horizontal distance from the beginning of the wave to the end of the wave. It can also be measured as the distance from one wave crest to the next wave crest, or one wave trough to the next wave trough. In acoustics, we can define wavelength as the distance between the two successive compressions or expansions [28].

As mentioned earlier, the compression and expansion of an acoustic wave result in pressure variations along the waveform. This pressure variation is the key process that causes the thermoacoustic phenomenon. These pressure variations can also be used to estimate the sound intensity. Eq. (2.10) outlines how the sound intensity, L, in decibels can be estimated from the pressure measurements at two points. The decibel (dB), or one-tenth of a bel, is twenty times the logarithm of the ratio of the sound pressure to a reference pressure. This unit measures sound pressure level, and is useful because the ear hears sounds exponentially. Eq. (2.10) outlines how L, the sound pressure level in units of decibels, is calculated using the measured sound pressure P to the reference pressure P_{ref}. P_{ref} is the pressure corresponding to the threshold of hearing and is 0.00002 N/m^2. As a sound wave registers more decibels, it sounds louder [28].

$$L = 20 \log_{10} P/P_{ref} \tag{2.10}$$

The equation indicates that larger the pressure variations, higher will be the sound intensity, or vise versa.

From the ideal gas equation of state,

$$\frac{P}{\rho} = RT \tag{2.11}$$

where P is the pressure, ρ is the density, T is the absolute temperature, and R is the gas constant. The above equation indicates that if the density variations are very small, the change in pressure causes the change in temperature. That is, an increase in pressure causes an increase in temperature and vice versa.

2.3 Thermodynamic Considerations

In this section, we will discuss the thermoacoustic phenomenon based on acoustics and thermodynamics. To understand the phenomenon, consider a thermoacoustic cooling device such as refrigerator. This device consists of an acoustic driver attached to an acoustic resonator (tube) filled with the working fluid. Inside the resonator tube, a stack of thin parallel plates and two heat exchangers (hot and cold) are installed for the heat transfer. The schematic of a typical thermoacoustic device is shown in Fig. 2.4(a).

The acoustic driver, connected to one end of the resonator tube, excites the working fluid (typically a gas with low Prandtl number), and creates a standing acoustic wave inside the tube. Hence the gas oscillates inside the resonator with expansions and compressions. For simplicity, the effect of viscosity and the longitudinal thermal conductivity in the gas are neglected. The length of the resonator tube is typically set equal to one-half of the wavelength of the standing wave, i.e. $\lambda/2$.

The standing wave creates velocity nodes at the two ends of the tube and a pressure node at the middle of the tube (see Fig. 2.4b). If a stack of parallel plates is placed inside the tube, the gas will be at a higher pressure at the end of the stack, which is closer to the end of the tube (i.e. left side of the stack in Fig. 2.4a), than the other end of the stack. This high pressure results in an increase in the temperature of the gas and the excess heat is transferred to the stack, causing an increase in the temperature of the stack at that end and an average longitudinal temperature gradient ∇T_m along the stack is established (see Fig.2.4c).

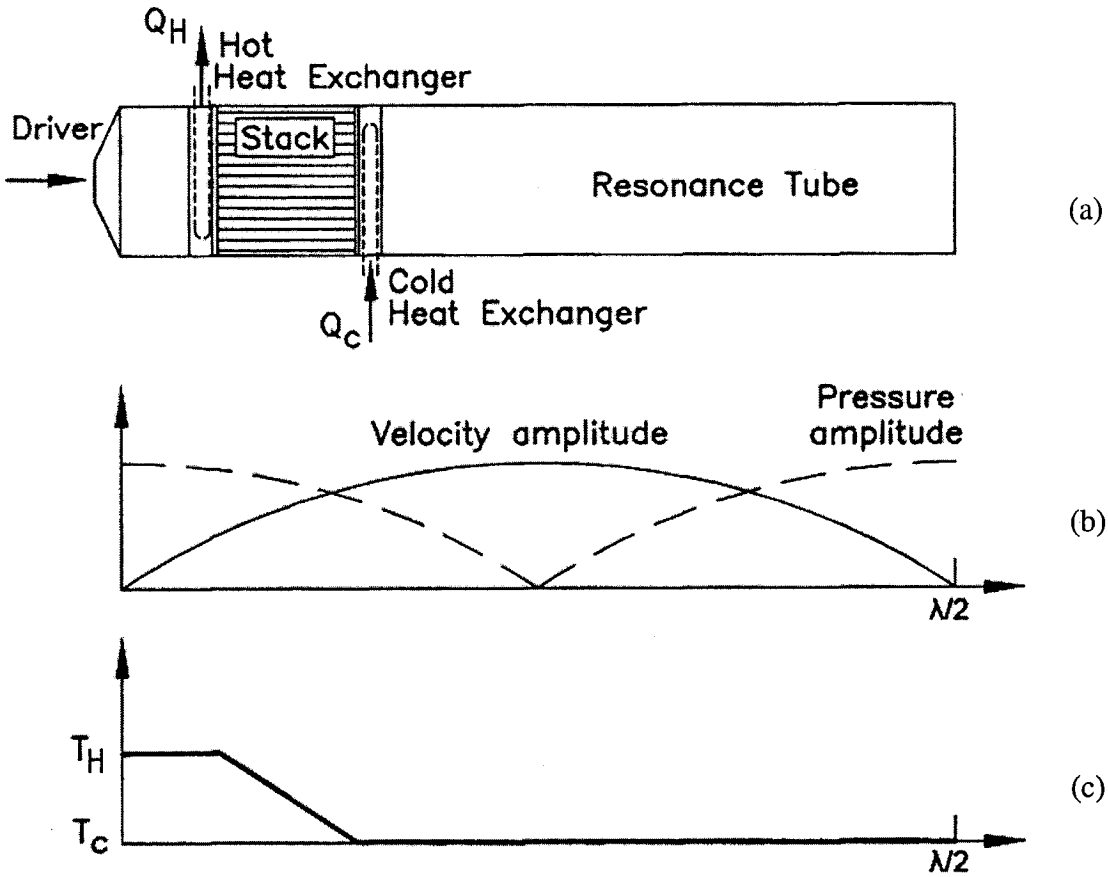

Figure 2.4: (a)Schematic of a thermoacoustic refrigerator. (b)The velocity and pressure variations across the resonance tube. (c)Temperature variation across the resonance tube.

2.3.1 Heat Transfer Mechanism inside the Stack

To understand the mechanism of heat transfer inside the stack under the influence of the acoustic wave (i.e. thermoacoustic phenomenon), consider the oscillation of a parcel (a small volume) of the working gas along a stack plate. A parcel of the gas (circular box) close to the cold end of a stack plate is shown in Fig. 2.5.

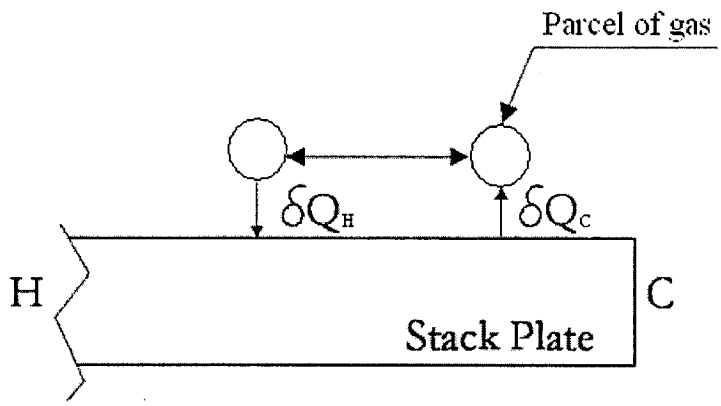

Figure 2.5: Heat transfer mechanism inside the stack.

The thermodynamic cycle of this gas parcel is shown in Fig. 2.6 . This cycle consists of four processes; adiabatic compression (from state A to B), constant pressure heat loss (from state B to C), adiabatic expansion (from state C to D), and constant pressure heat gain (from state D to A). At the beginning of the thermodynamic cycle i.e. state A, the gas parcel is close to the cold end of the stack and its temperature is T_A. During the first process, the parcel undergoes adiabatic compression, and it moves to the left (i.e. towards the pressure antinode). At the end of this process, its temperature rises to T_B. As a result, the gas parcel is warmer than the stack plate, and heat is irreversibly transferred to the stack plate during the second process by an amount δQ_H. At the end of

this process, the temperature of the gas parcel reduces to T_C. During the third process, the parcel undergoes adiabatic expansion as the gas parcel moves towards its initial spatial location and its temperature decreases to T_D. At the end of this process the gas parcel is cooler than the stack plate there. During the fourth process there is an irreversible heat transfer from the stack plate to the gas parcel by an amount δQ_C. As a result, the temperature of the gas parcel increases to its original temperature T_A. At the end of this process, the gas parcel completes one thermodynamic cycle and starts the cycle again. Thus, the sound wave inside the tube pumps heat from the cold end of the stack to the hot end and creates a temperature gradient across the stack as shown in Fig. 2.4(c).

Let the temperature, pressure and volume of the parcel of gas at point A (beginning of cycle) be:

$$T_A = T_m - X_1 \nabla T_m \tag{2.12}$$

$$P_A = P_m - P_1 \tag{2.13}$$

$$V_A = V \tag{2.14}$$

where T_m and P_m are the mean temperature and mean pressure of the gas and X_1 is half of the distance that the parcel of gas moves during the oscillation process and ∇T_m is the average longitudinal temperature gradient along the stack. P_A, V_A, T_A are the pressure, the volume and the temperature of gas parcel at the point A, respectively [26].

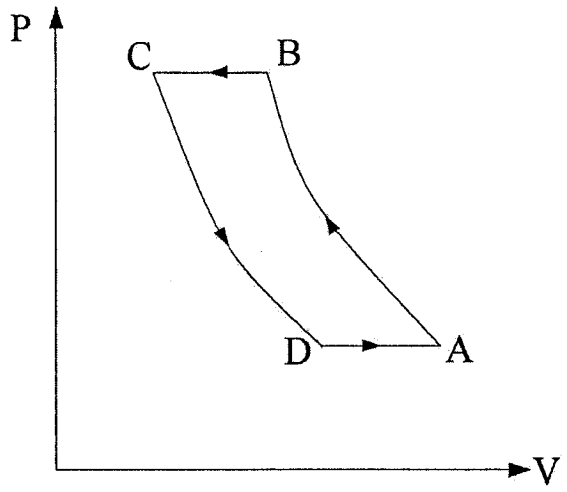

Figure 2.6(a): Thermodynamic cycle of the gas parcel plotted in pressure versus volume form.

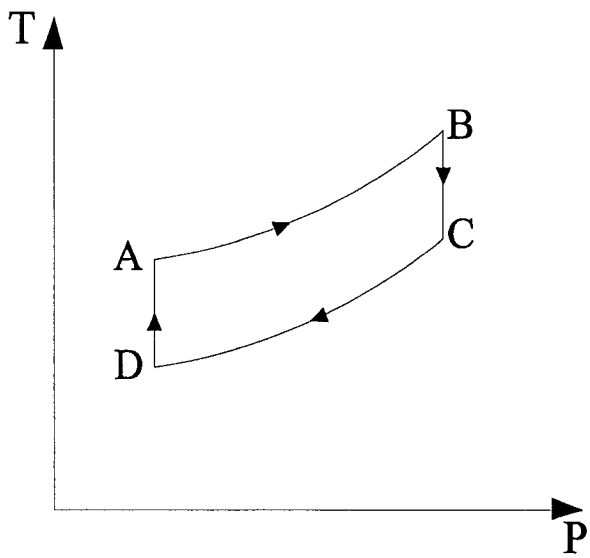

Figure 2.6(b): Thermodynamic cycle of the gas parcel plotted on a T-P diagram.

During the first process, the gas parcel moves a distance $2X_1$ towards left side of the resonator inside the stack, and the temperature and the pressure increase, and the volume decreases by $2T_1$, $2P_1$ and V_1 respectively. Using the laws of thermodynamics and the ideal gas relationships, the temperature can be expressed as,

$$\frac{T_1}{T_m} = \frac{\gamma - 1}{\gamma} \frac{p_1}{p_m} \tag{2.15}$$

where γ is ratio of isobaric to isochoric specific heats [29].

Similarly, the temperature, pressure and volume at the second state can be expressed by the following equations:

$$T_B = T_m - X_1 \nabla T_m + 2T_1 \tag{2.16}$$

$$P_B = P_m + P_1 \tag{2.17}$$

$$V_B = V - V_1 \tag{2.18}$$

where P_B, V_B, T_B are the pressure, the volume and the temperature of gas parcel at the point B.

The temperature difference between the gas parcel and the stack plate is given by:

$$\delta T = 2T_1 - 2X_1 \nabla T_m \tag{2.19}$$

where $2X_1 \nabla T_m$ is the temperature change along the stack plate [26].

The amount of heat δQ, that flows from the gas to the stack plate during the second process will be:

$$\delta Q = mc_p \delta T \tag{2.20}$$

The acoustic power input needed to transfer δQ in one cycle is given by,

$$\delta W \approx -2p_1(\beta V)_m \delta T \tag{2.21}$$

During the third process, the gas parcel moves towards pressure node, and as a result, the pressure decreases and the gas parcel cools off. At the beginning of third process (i.e. state C):

$$T_C = T_m + X_1 \nabla T_m \tag{2.22}$$

$$P_C = P_m + P_1 \tag{2.23}$$

$$V_C = V - V_1 - \delta V \tag{2.24}$$

where P_C, V_C, T_C are the pressure, the volume and the temperature of gas parcel at the point C.

In the fourth process, gas parcel is cooler than the stack plate and hence heat transfer from stack plate to gas parcel takes place. At the beginning of the fourth process (i.e. state D):

$$T_D = T_m + X_1 \nabla T_m - 2T_1 \tag{2.25}$$

$$P_D = P_m - P_1 \tag{2.26}$$

$$V_D = V - \delta V \tag{2.27}$$

where P_D, V_D, T_D are the pressure, the volume and the temperature of gas parcel at the point D.

If the temperature change of the stack plate ($2X_1\nabla T_m$) is exactly equal to the adiabatic temperature change during the adiabatic process ($2T_1$), then the temperature gradient in the stack is called the critical temperature gradient, which is given by:

$$(\nabla T)_{crit} = \frac{T_1}{X_1} \tag{2.28}$$

By combining Eq. (2.28), $T_1 = \left(\frac{\beta T}{\rho C_p}\right)_m p_1$, and $X_1 = \frac{u_1}{\omega}$ [26] ,we obtain:

$$(\nabla T)_{crit} = \frac{p_1 \omega}{\rho_m c_p u_1} \tag{2.29}$$

Using the critical temperature gradient to normalize the temperature gradient along the stack, results in [26]:

$$\Gamma = \frac{\nabla T_m}{(\nabla T)_{Crit}} \tag{2.30}$$

If $\Gamma < 1$, the heat is transferred from the cold end of the stack to the hot end (i.e. toward pressure antinode). The work in this case is also negative (i.e. the work is done on the system). In this case, the thermoacoustic device operates as a refrigerator. If $\Gamma = 1$, there is no heat flow and no work input is needed. When $\Gamma > 1$, the heat transfer is positive, and heat flows from the hot end of the stack to the cold end (i.e. towards the pressure node). The work is positive in this case, indicating that the work is done by the

system, that is, useful work output is produced by the device, and therefore the device operates as a prime mover [11].

The heat that is transferred by this parcel of the gas during one cycle is taken by the adjacent gas parcel on the higher-pressure side i.e. the gas parcel on the left side as shown in Fig. 2.7. This adjacent gas parcel goes through a similar thermodynamic cycle and delivers heat to the gas parcel located on its left side. This process continues until the heat is transferred to the hot-end of the stack [28]. If this cycle continues, the working gas keeps transferring heat from the end of the stack that is away from the pressure antinode i.e. the cold-end of stack (as shown in Fig. 2.7) to the other end of the stack (i.e. the hot-end of the stack close to the pressure antinode). As a result, a temperature gradient is established between the two ends of the stack [2].

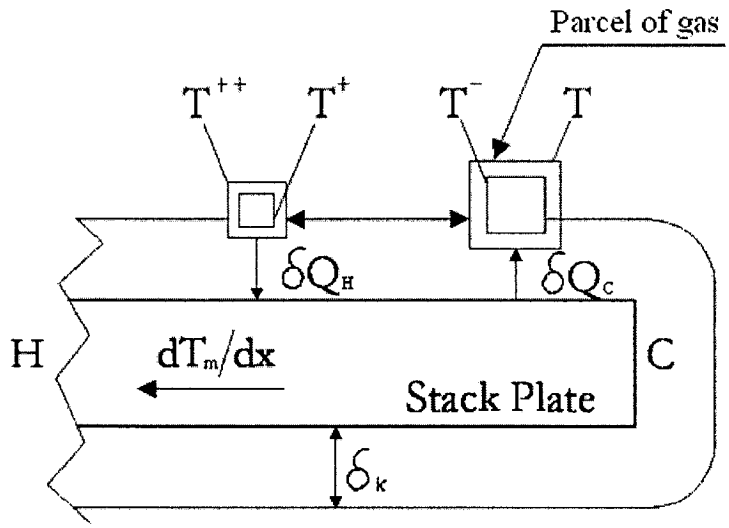

Figure 2.7: Magnified illustration of a stack plate and the elementary thermoacoustic cycle. The positive and negative superscripts on the temperature indicate the increase and decrease in temperature, respectively, from the initial temperature T [22].

2.3.2 Length Scales in Thermoacoustic Systems

In a thermoacoustic refrigerator, two characteristic length scales of the stack are important from the design considerations. One is called the thermal penetration depth, δ_k, and the other is called the viscous penetration depth, δ_v. The thermal penetration depth, δ_k corresponds to the thickness of the layer around the stack plate through which the heat can diffuse during a complete oscillating cycle of a gas parcel. It is defined as,

$$\delta_k = \sqrt{\frac{2K}{\rho C_p \omega}} \tag{2.31}$$

where, K is thermal conductivity of the gas, C_p is specific heat per unit mass at constant pressure, ρ is density of gas at the mean temperature(T_m), and ω is the angular velocity. That is, $\omega=2\pi f$, where f is the frequency of the acoustic wave.

The viscous penetration depth δ_v, is the thickness of the layer around the stack plate where the viscous effects are significant. It is defined as:

$$\delta_v = \sqrt{\frac{2\mu}{\rho\omega}} \tag{2.32}$$

Where μ is dynamic viscosity of the gas [27].

At a distance greater than the thermal penetration depth from the plate, the gas does not feel any thermal effects of the plate. In other words, the heat exchange between the gas parcel and the stack plate occurs only at a distance less than δ_k from the stack plate. The viscous effects are not desirable for the thermoacoustic process. The viscous effect decreases as the distance from the solid boundary (i.e. the stack plate) increases.

However, away from the solid boundary, the thermal contact between the gas and the stack plate decreases which reduces the thermoacoustic heat transfer. The viscous and thermal penetration depths are used to select the optimum lateral distance between the two stack plates. An optimum distance is the one when the viscous effect is minimum and the thermal contact is strong enough for the heat transfer. The square ratio of the viscous penetration depth to the thermal penetration depth is called the Prandtl number, σ [26],

$$\sigma = \left(\frac{\delta_v}{\delta_k} \right)^2 \tag{2.33}$$

The Prandtl number is close to unity for typical gases. For a thermoacoustic device, a gas with lower Prandtl number is used which has higher thermal effect and lower viscous effect.

It should be noted that in a thermoacoustic refrigerator, the gas displacement amplitude X_1, which is the ratio of the velocity amplitude $|u_1|$ to the angular velocity, ω of the wave, is much smaller than the acoustic wavelength and the stack horizontal length, and much larger than both penetration depths [26].

2.4 Theoretical Study of the Thermoacoustic Phenomenon

Thermoacoustics deals with the energy conversion processes, activated by the interaction of the temperature oscillations (accompanying the pressure oscillations) in a sound wave, with the solid boundaries. The theory of thermoacoustics is mainly based on basically a low amplitude linearization of the Navier-Stokes equation with sinusoidal oscillations of all variables as reported by Rott and co- workers in 1980 [29]. The steady-state sinusoidal oscillations of variables such as pressure, temperature, entropy, and

density are considered in the analysis. Mean values of the variables are considered to be spatially uniform, i.e. independent of x, y, and z. These variables are expressed in the complex notation as:

$$p = p_m + \mathrm{Re}[p_1(x)e^{i\omega t}] \tag{2.34}$$

$$u = \mathrm{Re}[u_1(x, y, z)e^{i\omega t}] \tag{2.35}$$

Similarly for y and z components:

$$T = T_m + \mathrm{Re}[T_1(x, y, z)e^{i\omega t}] \tag{2.36}$$

$$\rho = \rho_m + \mathrm{Re}[\rho_1(x, y, z)e^{i\omega t}] \tag{2.37}$$

$$s = s_m + \mathrm{Re}[s_1(x, y, z)e^{i\omega t}] \tag{2.38}$$

Recognizing that $\frac{\partial}{\partial x}$ tends to be of the order of $\frac{1}{\lambda}$ while $\frac{\partial}{\partial y}$ tends to be of the order of $\frac{1}{\delta_v}$ and $\frac{1}{\delta_k}$, $\frac{\partial}{\partial x}$ can be neglected in comparison to $\frac{\partial}{\partial y}$ and $\frac{\partial}{\partial z}$ [27].

The governing thermoacoustic equations are derived from the linearized Navier-Stokes, continuity, and energy equations, and using the second law of thermodynamics (entropy balance). The first governing equation is called Rott's wave equation, which is the wave equation for the pressure when the temperature gradient along the stack exists. The second governing equation is the time-average energy flux equation, and the third governing equation is called the acoustic power equation that can be used to derive the acoustic power absorbed in the stack.

The following assumptions have been made to obtain the governing equations [27].

1. Viscosity does not change for small temperature changes.
2. The oscillating pressure varies only along the x-axis, that is, $p = p\ (x)$.
3. Second order terms for acoustic streaming and turbulence are neglected.
4. Subscript 1 is used to show first order and the usual complex notations for the time-oscillating quantities (pressure p, temperature T, velocity components, density ρ, and entropy per unit mass s) are used in this chapter. It is assumed that this lowest order in the acoustic amplitude suffices for all variables.

All four fundamental equations are given below.

The Navier-Stokes equation:

$$\rho\left[\frac{\partial V}{\partial t}+(V\cdot\nabla)\ V\right]=-\nabla p+\nabla\cdot\sigma' \tag{2.39}$$

The continuity equation:

$$\frac{\partial\rho}{\partial t}+\nabla\cdot(\rho V)=0 \tag{2.40}$$

The energy equation:

$$\frac{\partial}{\partial t}\left(\rho\varepsilon+\frac{1}{2}\rho|V|^2\right)=-\nabla\cdot\left[\rho V\left(\frac{1}{2}V^2+h\right)-K\nabla T-V\cdot\sigma'\right] \tag{2.41}$$

The entropy equation:

$$\rho T\left[\frac{\partial s}{\partial t}+(V\cdot\nabla)\ s\right]=\nabla\cdot K\nabla T+(\sigma'\cdot\nabla)\cdot V \tag{2.42}$$

where ρ is density, V is velocity, σ' is nine-component viscous stress tensor, p is pressure, K is gas thermal conductivity, ε is internal energy per unit mass, h is internal enthalpy per unit mass [27].

The governing equations obtained from the fundamental equations are,

Rott's wave equation:

$$\left[1+\frac{(\gamma-1)}{(1+\varepsilon_s)}f_k\right]p_1+\frac{a^2}{\omega^2}\rho_m\frac{d}{dx}\left[\frac{(1-f_v)}{\rho_m}\frac{dp_1}{dx}\right]+\frac{a^2}{\omega^2}\frac{(f_k-f_v)}{(\sigma-1)(1+\varepsilon_s)}\beta\frac{dT_m}{dx}\frac{dp_1}{dx}=0 \tag{2.43}$$

where f_k and f_v are called Rott's functions and includes thermal and viscous effects, respectively, and they are geometry dependent [27].

Total power:

$$E_2=-\frac{1}{4}\Pi\delta_k\frac{\beta T_m p_{s1}\langle u_{s1}\rangle}{(1+\sigma)(1+\varepsilon_s)\Lambda}\left(\Gamma\frac{1+\sqrt{\sigma}+\sigma(1+\varepsilon_s)}{1+\sqrt{\sigma}}-\left(1+\sqrt{\sigma}-\frac{\delta_v}{y_0}\right)\right)-\Pi(y_0K+lK_s)\frac{dT_m}{dx} \tag{2.44}$$

where,

$$\Lambda=1-\frac{\delta_v}{y_0}+\frac{\delta_v^2}{2y_0^2} \tag{2.45}$$

and,

$$p_1=p_{s1}=p_0\cos(kx) \tag{2.46}$$

and,

$$\langle u_1 \rangle = i\langle u_{s1} \rangle = i(1+\frac{l}{y_0})\frac{p_0}{\rho_m a}\sin(kx) \tag{2.47}$$

and,

$$(\nabla T)_{crit} = \frac{\beta T_m p_{s1}\omega}{\rho_m c_p \langle u_{s1} \rangle} \tag{2.48}$$

and,

$$\Pi = \frac{A}{y_0 + l} \tag{2.49}$$

where L_s is the stack length, Π is the total perimeter of the stack plates in the direction normal to the x axis, k is the wave number ($2\pi/\lambda$.), p_0 is the pressure amplitude at the pressure antinodes of the standing wave [27].

The first term on the right hand side of Eq. (2.44) is the thermoacoustic heat flow and the second term is simply the conduction of heat through gas and stack material in the stack region.

Acoustic power:

$$W_2 = \left(\frac{1}{4}\Pi\delta_k L_s \frac{(\gamma-1)\omega(p_{s1})^2}{\rho_m a^2(1+\varepsilon_s)}\right)\left(\frac{\Gamma}{(1+\sqrt{\sigma})\Lambda}-1\right) - \frac{1}{4}\Pi\delta_v L_s \frac{\omega\rho_m\langle u_{s1}\rangle^2}{\Lambda} \quad (2.50)$$

The term in the first bracket and the second term in the Eq. (2.50) are the thermal and viscous relaxation dissipation terms, respectively. These two terms have a dissipative effect on the performance of thermoacoustic devices [27].

In this chapter basic refrigerator theory, acoustic theory, thermoacoustic consideration and theoretical study of thermoacoustic refrigerator are explained. Numerical study, designing and selecting of the thermoacoustic refrigerator components will be explained in the next chapter.

Chapter 3

Design Considerations

This chapter deals with the design, development and optimization of the thermoacoustic refrigerator. The linear thermoacoustic theory presented in chapter 2 will be used for the design analysis. Due to the large number of parameters, a choice of some parameters along with a group of dimensionless independent variables will be used. The optimization of the different parts of the refrigerator will be discussed, and likewise some criteria will be implemented to obtain an optimal system.

3.1 Numerical Study

In order to develop a thermoacoustic refrigerator, a numerical study is conducted first. The simulation of the flow was performed to obtain the important design parameters. The important parameters involved in the design of a thermoacoustic refrigerator are listed in Table 3.1.

A thermoacoustic cooling device such as refrigerator consists of an acoustic driver attached to the acoustic resonator (tube) filled with a working fluid. Inside the resonator tube, a stack of thin parallel plates and two heat exchangers (hot and cold) are installed (see Fig. 3.1).

Mean temperature of the gas:	T_m	Mean pressure of the gas:	P_m
Dynamic pressure amplitude of the gas:	P_o	Frequency:	f
Drive Ratio:	D= P_o / P_m	Temperature difference between	
Kinematic viscosity:	ν	the two sides of stack:	ΔT_m
Thermal conductivity:	K	Prandtl number:	σ
Sound velocity:	a	Specific heats ratio:	γ
Blockage Ratio:	B		

Table 3.1: A list of important design parameters.

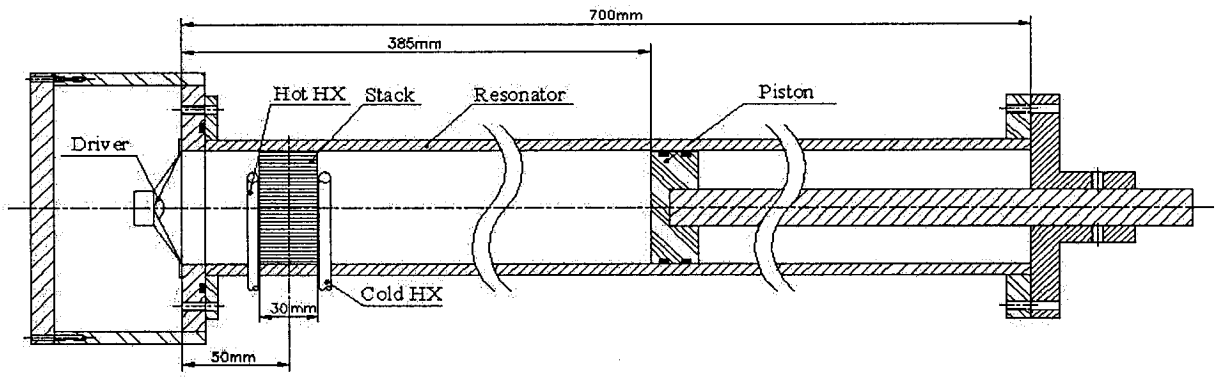

Figure 3.1: Schematic of the thermoacoustic refrigerator.

Some of the design parameters used in the present study are tabulated in Table 3.2.

P_m=1 atm	D=0.013	σ = 0.7
T_m=300 K	a =345 m/s	B =0.735
ΔT_m=25 K	γ =1.4	

Table 3.2: The design parameters for the present study.

3.2 Acoustic Driver

The total acoustic power used by the refrigerator is provided by an acoustic driver. A significant portion of this power is used to pump heat in the stack and the rest is dissipated in different parts of the refrigerator. A higher performance of the driver leads to a higher performance of the whole refrigerator system. The Acoustic driver converts electric power input to the acoustic power. The most common loudspeaker is of electrodynamic type which uses copper wires and permanent magnets. A loudspeaker with the maximum power of 15 watts, and 8 Ω at the operating frequency of 450 Hz was selected as the acoustic driver for this study.

3.3 Acoustic Resonator

The shape, length, weight and the losses are important parameters for designing the resonator. Length of resonator is determined by the resonance frequency and minimal losses at the wall of the resonator. The length of resonator tube corresponds to half the wavelength of the standing wave;

$$L = \lambda/2 \tag{3.1}$$

and

$$\lambda = a/f \tag{3.2}$$

where, a is the speed of sound, λ is the wavelength and f is the resonance frequency.

The viscous and thermal relaxation dissipation losses take place within the distance equal to the penetration depths, from the surface of the resonator. The acoustic power lost per unit surface area of the resonator is obtained from Eq. 2.50 by setting Γ=0 and is given b,

$$\frac{dW_2}{dS} = \frac{1}{4}\rho_m \left|\langle u_1 \rangle\right|^2 \delta_v \omega + \frac{1}{4}\frac{|p_1|^2}{\rho_m a^2}(\gamma - 1)\delta_k \omega \qquad (3.3)$$

where the first term on the right hand side is the kinetic energy dissipated by viscous shear. The second term is the energy dissipated by thermal relaxation. The total dissipation energy is proportional to the surface area of the resonator [26].

As discussed in section 3.2, an acoustic driver with the resonance frequency of 450 Hz was selected for the present design. For this resonance frequency the length of the resonant tube was set equal to 385 mm that corresponds to the half wavelength of the acoustic standing wave, the diameter of the resonator tube was set equal to 63 mm to accommodate the size of the acoustic driver (see Fig. 3.1).

3.4 Stack Optimization

The most important component of a thermoacoustic device is the stack inside which, the thermoacoustic phenomenon occurs. Thus, the characteristics of the stack have a significant impact on the performance of the thermoacoustic device. The stack material should have good heat capacity but low thermal conductivity. The low thermal conductivity for the stack material is necessary to obtain high temperature gradient across the stack and a heat capacity C_s larger than the heat capacity of the working fluid. In

addition, the stack material should minimize the effects of viscous dissipation of the acoustic power [17].

There are different geometrical configurations of stack pores such as; parallel plates, circular, hexagonal and square pin arrays. These geometries are used to have efficient thermal contact between the working fluid and the solid surface across the cross-sectional area. The pin array and parallel-plates stack have shown to be the best geometries [26]. Numerical studies confirm that efficiency and power are almost 10%-20% more with parallel-sided channel than honeycomb channel. The best location to put stack inside the resonator is about $\lambda/20$ from the nearest velocity node [27]. Stack should be chosen from among materials with the smallest possible thermal conductance in order to prevent the reduction of temperature gradient along the stack. In this project, a spiral stack that can be considered as a stack with parallel-plate geometry is used. Using Eqs. (2.31) and (2.32), we have computed the thermal and viscous penetration depths for our system, i.e. $\delta_k = 0.126$ mm and $\delta_v = 0.106$ mm. The optimal value for spacing between the stack layers is $2\delta_k$ to $4\delta_k$ [17]. The spacing between the stack layers ($2y_0$) is set equal to 0.36 mm. The distance between the two plates is set in a way that the gas between the two plates remains in thermal contact with the surface of either of the two plates, with the minimum possible viscous effect. The distance between the two layers is set larger than the thermal and viscous penetration depths for the design condition.

3.4.1 Stack Design Parameters

There are three main stack design parameters which are normalized stack position (X_{sn}), normalized stack length (L_{sn}), and the stack cross-sectional area (A). Typically, the

resonator tube cross-sectional area is equal to the stack cross-sectional area. The dimensionless parameters, X_{sn}, and $L_{sn,}$, are defined as,

$$X_{sn} = \frac{2\pi f}{a} X_s \tag{3.4}$$

$$L_{sn} = \frac{2\pi f}{a} L_s \tag{3.5}$$

where, L_s is the length of the stack and X_s is the distance from the mid length of stack to the nearest end of the resonator tube. Some other normalized parameters used in the design of the stack are;

$$\Delta T_{mn} = \frac{\Delta T_m}{T_m} \tag{3.6}$$

$$\delta_{kn} = \frac{\delta_k}{y_0} \tag{3.7}$$

where ΔT_m is temperature difference across the two ends of stack, T_m is the mean air temperature inside the resonator tube, ΔT_{mn} is the normalized temperature difference, δ_k is thermal penetration depth, and y_o is half of the spacing length between the stack layers, and δ_{kn} is the normalized thermal penetration depth.

For the ideal gas and ideal stack, the stack material can be chosen so that ε_s (stack heat capacity ratio) and thermal conductive term in Eqs. (2.44.) and (2.50) can be neglected. Hence Eqs. (2.44) and (2.50) can be written in a dimensionless form by using the dimensionless parameters, the gas data of Table 3.1, and ε_s=0 as

$$Q_{Cn} = \frac{Q_C}{P_m aA} = -\frac{\delta_{kn} D^2 \sin(2X_{sn})}{8\gamma(1+\sigma)(1-\sqrt{\sigma}\delta_{kn}+\frac{1}{2}\sigma\delta_{kn}^2)} \times (\frac{\Delta T_{mn} \tan(X_{sn})}{(\gamma-1)B \times L_{sn}} \times \frac{(1+\sqrt{\sigma}+\sigma)}{1+\sqrt{\sigma}} - (1+\sqrt{\sigma}-\sqrt{\sigma}\delta_{kn})) \tag{3.8}$$

$$W_n = \frac{W}{p_m aA} = \frac{\delta_{kn} D^2 L_{sn} (\gamma - 1) B \cos^2(X_{sn})}{4\gamma} \times (\frac{\Delta T_{mn} \tan(X_{sn})}{BL_{sn}(\gamma - 1)(1 + \sqrt{\sigma})(1 - \sqrt{\sigma}\delta_{kn} + \frac{1}{2}\sigma\delta_{kn}^2)} - 1) - \frac{\delta_{kn} L_{sn} D^2}{4\gamma} \times \frac{\sqrt{\sigma} \sin^2(X_{sn})}{B(1 - \sqrt{\sigma}\delta_{kn} + \frac{1}{2}\sigma\delta_{kn}^2)} \tag{3.9}$$

where Q_{Cn} is the normalized cooling power, W_n is the normalized acoustic power and B is the blockage ratio defined as the fraction of the cross sectional area of the resonator blocked for the gas movement by the stack plates [17].

The stack geometry parameters can be optimized by optimizing the coefficient of performance (COP_{st}), which is defined as the ratio of the heat transferred from the cold end of the stack to the acoustic power input at the stack, that is:

$$COP_{st} = \frac{Q_C}{W} = \frac{Q_{Cn}}{W_n} \tag{3.10}$$

Using Eqs. (3.8), (3.9) and the design parameters in Table 3.2, the stack design parameters can be obtained.

An important parameter to be considered in the stack design is the temperature difference between the two ends of the stack, ΔT_m. Optimization is done based on 25 K temperature difference between the two ends of the stack.

After the temperature difference across the stack is selected, the next task is to determine the normalized length of the stack, L_{sn}, based on the value of X_{sn}, the normalized stack position. The COP_{st} is plotted against the normalized stack length for different stack positions in Fig. 3.2. The plot shows that as X_{sn} decreases, (i.e. the stack moves closer to the end of the resonator tube), the COP_{st} increases. For any specific value of X_{sn}, there is an optimum value of L_{sn}. The COP_{st} decreases as we increase or decrease the stack length from the optimum value. The highest value of COP_{st} is obtained if the stack length is very small and the stack is placed very close to the end of the resonator tube. Again, based on the fabrication considerations, it was decided to set X_{sn} = 0.42, although the COP_{st} was not the highest at this value. Fig. 3.3 shows the plot of COP_{st}, Q_{Cn} and W_n, against L_{sn} for X_{sn} = 0.42, and ΔT_m = 25 K. Based on the results in Fig. 3.3, the optimum normalized stack length, is chosen as L_{sn} =0.244.

The optimum values for the actual stack length, L_s, and the actual stack position, X_s, can be calculated by using Eqs. (3.4) and (3.5). For the selected values of L_s and X_s, the corresponding values are; L_s=3 cm and X_s =5 cm, respectively.

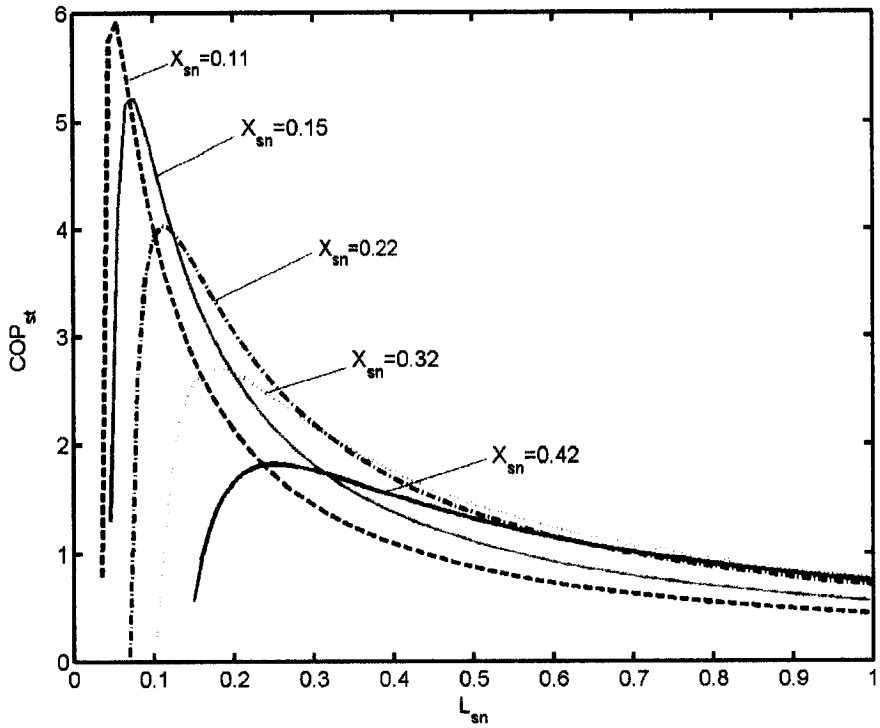

Figure 3.2: The COP_{st} versus the normalized stack length for different values of the normalized stack position. The values are computed at ΔT_m=25 K.

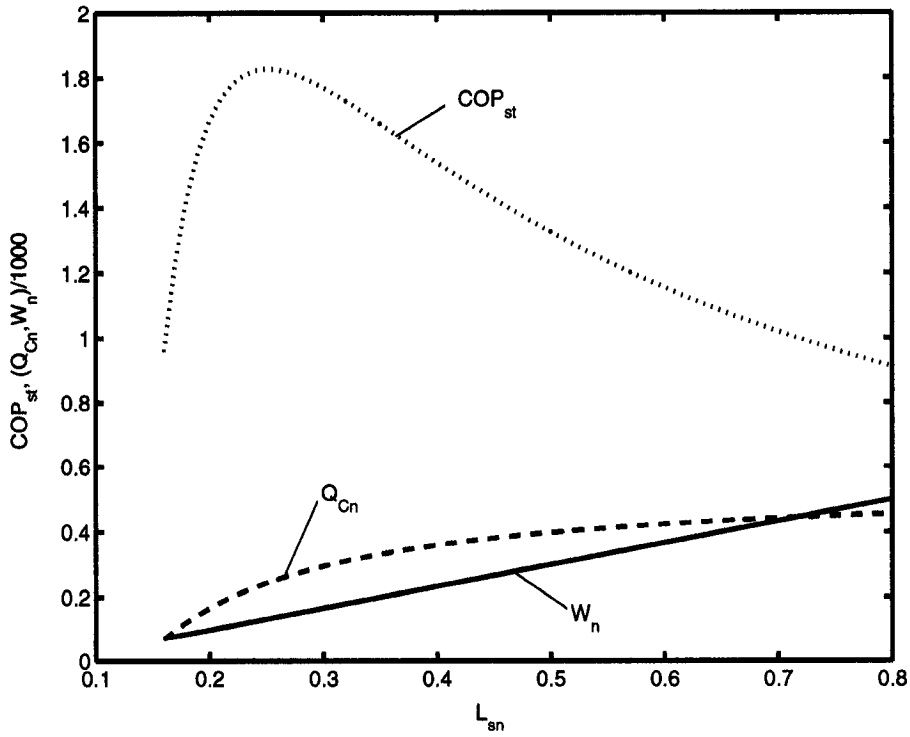

Figure 3.3: The COP_{st}, Q_{Cn} and W_n, versus L_{sn} for X_{sn} = 0.42, and ΔT_m = 25 K.

Although ΔT_m=25 K is selected, it was important to see the effect of ΔT_m on different design parameters. Simulations were performed for different values of ΔT_m to investigate the effect of ΔT_m on the design of the stack and the performance of the thermoacoustic refrigerator. The normalized acoustic power input corresponding to maximum COP_{st} is marked against the normalized stack length for four different values of ΔT_m in Fig. 3.4. These optimum points show that the normalized acoustic power and the normalized length of the stack increase as the temperature difference increases. As ΔT_m increases by a factor of five from 5 K to 25 K, both the normalized acoustic power and the normalized stack length increases approximately by the same factor of five.

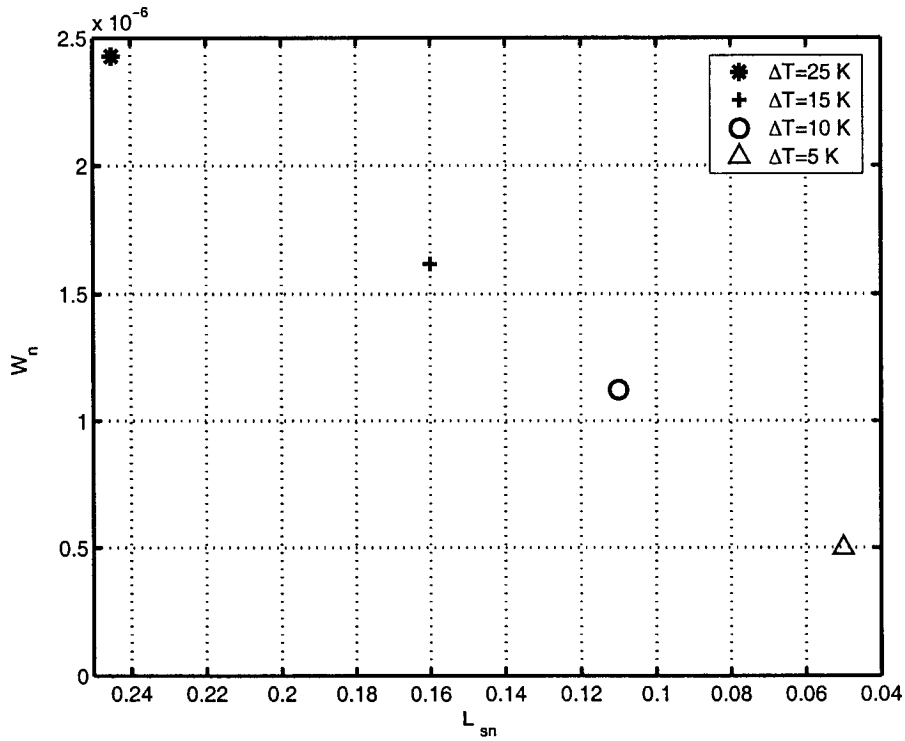

Figure 3.4: The normalized acoustic power, W_n, at the normalized stack position of X_{sn} = 0.42, versus the normalized length, L_{sn}, for four values of ΔT_m (temperature difference between the two sides of the stack).

The normalized cooling power, that is, the rate of heat transfer from the cold end of the stack, Q_{Cn}, is corresponding to optimum COP_{st} marked against the normalized stack length at different values of ΔT_m in Fig. 3.5. These optimum points show that as ΔT_m decreases from 25 K to 10 K, the cooling power increases by approximately 16%. Further decrease in ΔT_m results in a decrease in the cooling power

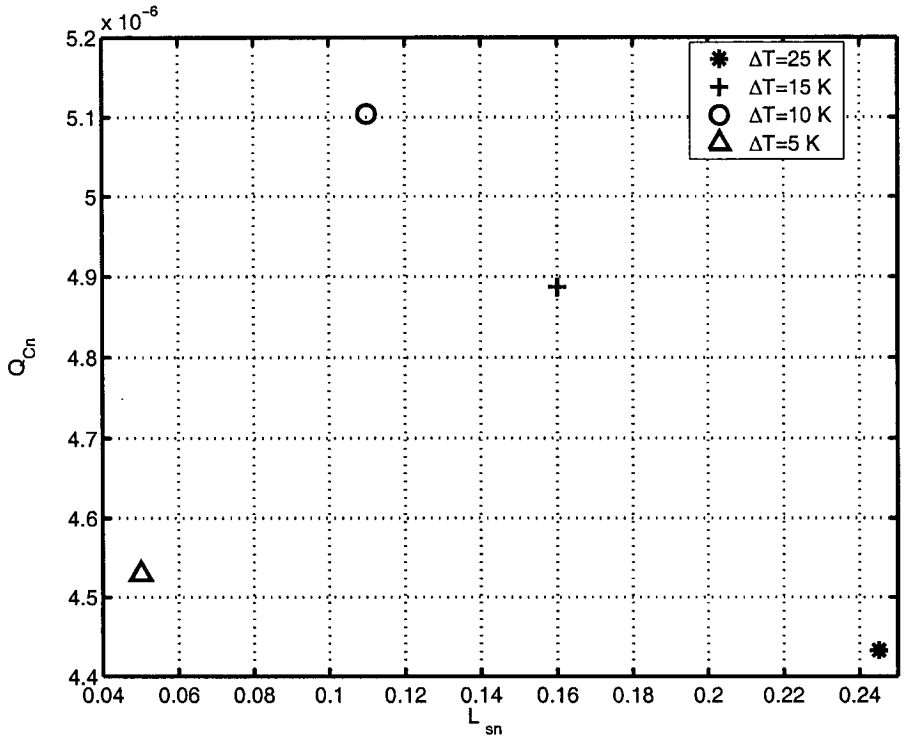

Figure 3.5: The normalized cooling power at the normalized stack position of X_{sn} = 0.42, versus the normalized stack length, for different temperature differences.

In order to analyze the impact of ΔT_m on the overall performance of the thermoacoustic refrigerator, the COP_{st} is plotted in Fig. 3.6 as a function of the normalized stack length for different values of ΔT_m. The plot shows that the COP_{st} increases as ΔT_m decreases. In order to get the highest cooling power, that is, the maximum heat transfer from the cold end of the stack, for the given four values of ΔT_m, the better value of ΔT_m is 10 K as Q_{Cn} at this temperature is greater than that at 5 K (see Fig. 3.5). However the physical length of the stack for ΔT_m = 10 K is 13 mm. This length of the stack is not suitable from the fabrication point of view. Based on the feasibility from the fabrication point of view and the objectives of this study, ΔT_m = 25 K was chosen. The stack length at this temperature difference is equal to 30 mm.

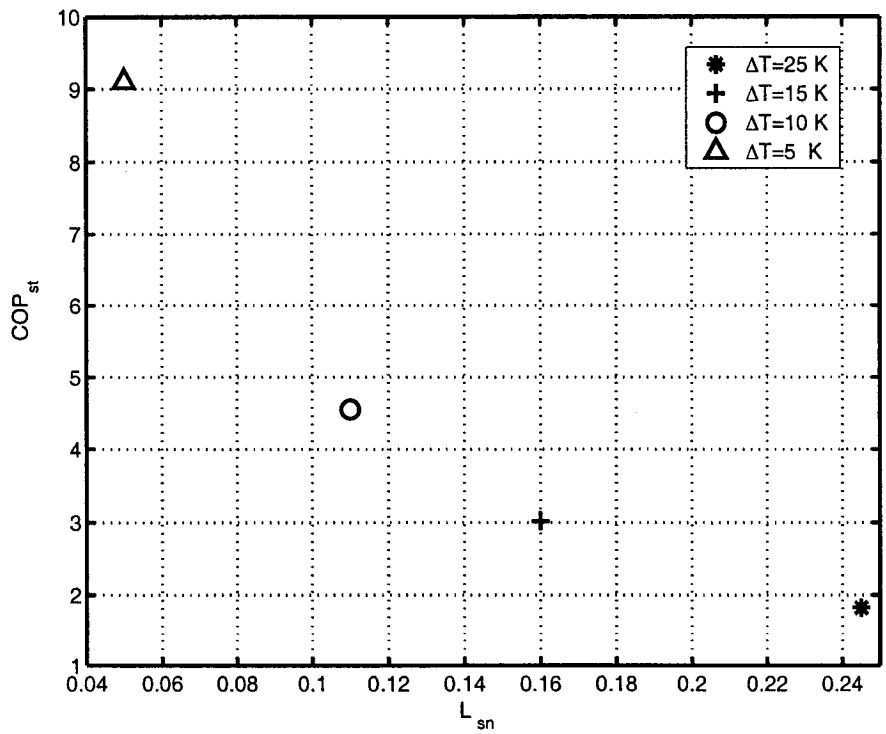

Figure 3.6: The COP_{st} plotted as a function of the normalized stack length, X_{sn} = 0.42, for different values of ΔT_m.

3.5 Heat Exchangers

In order to exploit the thermoacoustic effect for heat pumping; heat exchangers are attached at both ends of the stack. Heat exchangers transfer heat from the gas to the external sink or to the gas from an external source of heat. The design of the heat exchangers is a critical task in thermoacoustical systems. The heat transfer in oscillating flows with zero mean velocity is poorly understood. For the present study, the heat exchangers were designed with the following specifications.

- Material; Copper.
- Length; 12 cm.
- Tube outer diameter; 3/16 inch.
- Tube wall thickness; 0.03 inch.

In order to get more contact surface between the stack and the copper tube, it has been bent in the form of "M" (see Fig. 3.7).

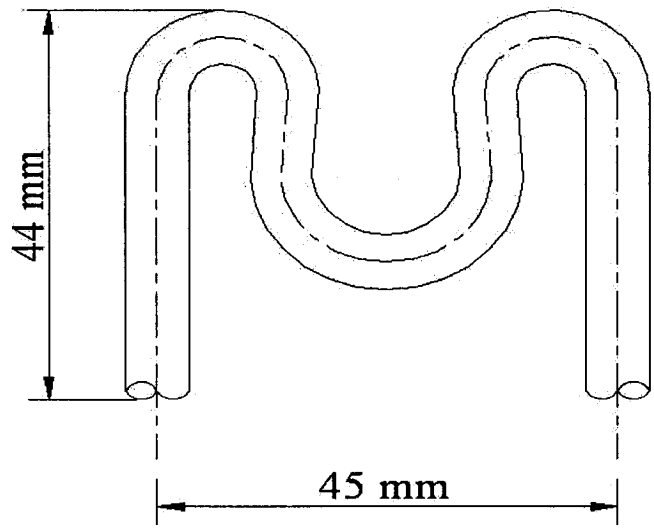

Figure 3.7: Schematic of cold and hot heat exchangers.

3.6 Working Fluid

Many parameters such as power, efficiency, and convenience are involved in the selection of the working fluid, and it depends on the application and objective of the device. Thermoacoustic power increases with an increase in the mean pressure inside the resonator. It also increases with an increase in the velocity of sound in the working fluid. The lighter gases such as H_2, He, Ne have the higher sound velocity. Lighter gases are necessary for the refrigeration application because heavier gases condense or freeze at low temperatures, or exhibit non ideal behavior. In order to obtain high efficiency and high power, a working gas with low Prandtl number and high sound speed should be chosen [26]. Air at atmospheric pressure is chosen as a working fluid for the present study.

3.7 DeltaE Software

DeltaE "Design Environment for Low-Amplitude ThermoAcoustic Engine" is a computer program that was developed by the research group at the Los Alamos National Laboratory [31]. This software solves the one-dimensional wave equation based on the low-amplitude, 'acoustic' approximation. It solves the wave equation for a gas or liquid, in a geometry given by the user.

The software can predict how a given thermoacoustic device will perform, or can allow the user to design a device to achieve the desired performance. DeltaE is a useful to tools for the researchers in physical acoustics, especially thermoacoustics. It is capable of handling complex geometrical configurations and specialized acoustic elements including resonators, duct networks, and complete thermoacoustic engines such as prime movers or

electroacoustically-driven refrigerators. The software can be downloaded free of cost from the website of the thermoacousric research group at the Los Alamos National Laboratory [31].

I the presented study, simulations were performed using the DeltaE software for the design and operating conditions discussed previously.

Volume flow rate against the resonator tube is plotted in Fig. 3.8. The plot shows that the maximum flow rate occurs at the middle of the resonator (L=0.19 m) and is minimum at both ends of the resonator. The volume flow rate at the left end is not zero because the loudspeaker is attached at this end and the velocity is not zero at the end due to the oscillation of the speaker diaphragm. At the solid end (i.e. the right end) the velocity and hence the flow rate is zero, as expected. The location of the stack is also shown in Fig. 3.8. The plot indicates that the volume flow rate at the cold end is greater than that at the hot end. The plot also shows that the volume flow rate does not change by varying the temperature difference across the stack.

The temperature inside the resonator is plotted versus the resonator length in Fig. 3.9 for different values of stack temperature gradient. The plot shows that the temperature on the cold side of the resonator tube is constant and equal to the temperature at the cold end of stack and temperature on the hot side of the resonator is constant and equal to the temperature at the hot end of the stack.

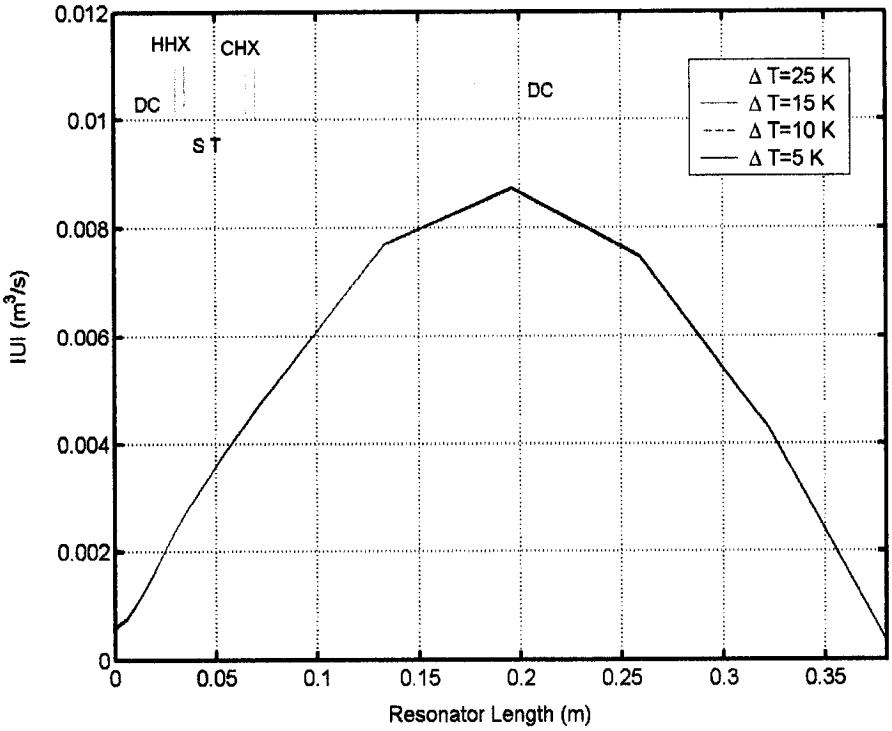

Figure 3.8: Volume rate gradient along the resonator tube at different values of ΔT_m. ST: stack, DC: resonator, HHX: hot heat exchanger, CHX: cold heat exchanger.

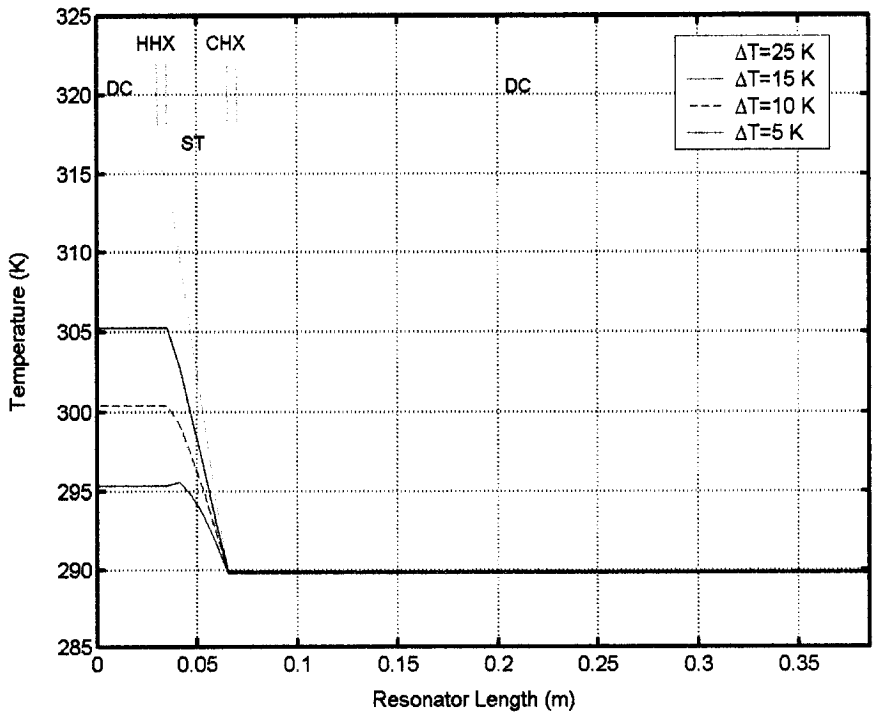

Figure 3.9: Temperature gradient along the resonator tube.

The pressure amplitude is plotted against the length of the resonator tube in Fig 3.10. The plot shows that the minimum pressure exists at the middle of the resonator and the maximum pressure (1250 Pa) is observed at the solid end and 1160 Pa at the loudspeaker end. As shown, the stack is placed between the pressure antinode and velocity antinode where both pressure and velocity are non-zero. The plot also shows that the pressure of the gas at the cold-end of the stack is lower than the pressure of the gas at the hot-end. Thus, as described by the thermoacoustic theory, the gas is compressed at the hot-end and expanded at the cold-end. The plot also shows that the pressure value inside the resonator tube does not vary significantly by changing the stack temperature difference.

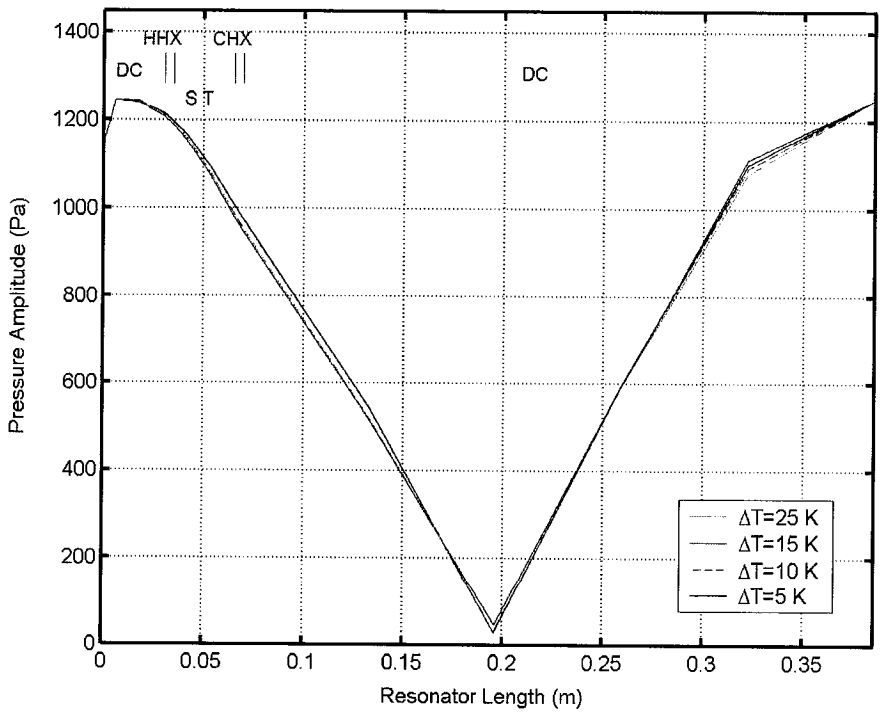

Figure 3.10: Pressure amplitude gradient along the resonator tube.

In this chapter, the designing of the acoustic driver, acoustic resonator, stack and heat exchangers is performed. A loudspeaker as acoustic driver, a piece of acrylic tube with 63 mm inner diameter as a resonator tube, two pieces of copper tube as heat exchangers, and stack built of mylar sheet with 3cm wide have been selected and optimized. The effect of the stack temperature difference on the performance of the thermoacoustic refrigerator was investigated using the analytical solution and the simulations from the DeltaE software. The results shows that the stack temperature difference does not affect the pressure and velocity (or volume flow rate) distribution inside the resonator. However, the *COP*, acoustic work and cooling load changes with the change in the stack temperature difference. In the next chapter, the development of the actual components of the thermoacoustic refrigerator based on the design presented in this chapter, are discussed. Also, the experimental setup and experiments will be described and the methods for acquiring the data and measurement will be explained.

Chapter 4

Fabrication and Experimental Setup

The components of the thermoacoustic refrigerator are designed, and the many design parameters are selected in the previous chapter. In this chapter, the fabrication of the thermoacoustic refrigerator is described, which is followed by the description of the experimental setup, instrumentation and methods for the measurements in the fabricated refrigerator.

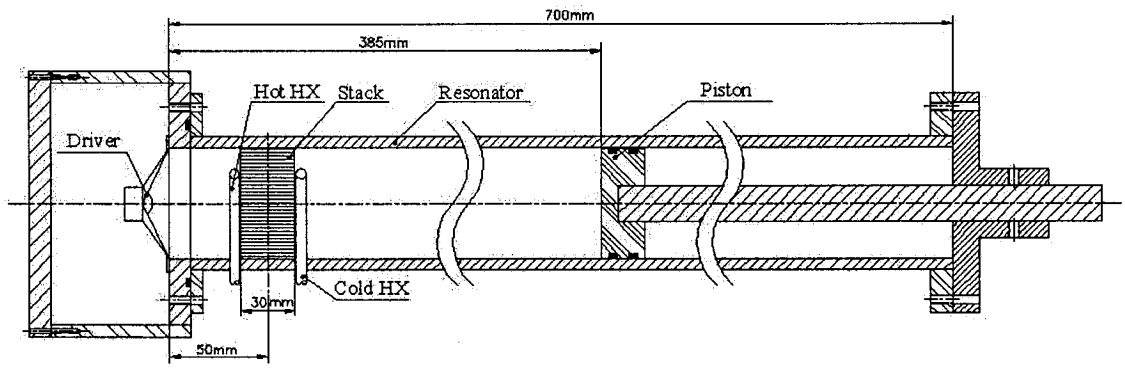

Figure 4.1: Schematic of the thermoacoustic refrigerator.

4.1 Fabrication

Based on the design and selection described in chapter 3, some standard components of the thermoacoustic refrigerator were purchased and some were fabricated. The details of each component is described below (see Fig. 4.1).

4.1.1 Acoustic driver

A thermoacoustic cooling device requires an acoustic driver attached to one end of the resonator, in order to create an acoustic standing wave in the gas at the fundamental resonant frequency of the resonator. The acoustic driver converts electric power to the acoustic power. In this study, a loudspeaker with the maximum power of 15 watts, and impedance of $8\,\Omega$ at the operating frequency (450 Hz) was used as the acoustic driver (G 50 FFL, VISATON). The loudspeaker was driven by a function generator and a power amplifier to provide the required power to excite the working fluid inside the resonator. Efficiency of this type of loudspeaker is relatively low, and their impedances are poorly matched to gas when the pressure inside the resonator is high. Consequently, the range of pressure amplitudes inside the resonator is limited [27].

4.1.2 Acoustic Resonator

The acoustic resonator was built from a straight acrylic tube of length 70 cm. The internal diameter of the tube was 6.3 cm and the wall thickness was 6 mm. One end of the tube has a plate attached to install the speaker frame. At the other end, a movable piston was placed inside the resonator. The reason for having a movable piston was to adjust the length of resonator so as to change the fundamental resonant frequency of the resonator (see Fig. 4.1). In the present design the resonance frequency of the resonator is 450 Hz. Thus, the length of resonator tube was set equal to 38.5 cm that corresponds to the half-wavelength of the acoustic standing wave generated at this frequency. The resonator was sealed at both ends with the rubber O-rings to minimize the sound energy leakage.

4.1.3 Stack

In this project, a spiral stack with parallel-plate geometry was used. The stack was made from the mylar sheet of thickness 0.13 mm. The mylar sheet was cut into pieces, each 3 cm wide. The spacing between the layers was realized by fishing line spacers (0.36 mm thick) glued onto the surface of the sheet. The distance between the two layers, i.e. 0.36 mm, was set larger than the thermal and viscous penetration depths for the design condition (see the thermal and viscous penetration depths computed in Chapter 3, section 2.3.2). The mylar sheet was wound around a 4 mm PVC-rod to obtain a spiral stack as shown in Fig. 4.2 [3].

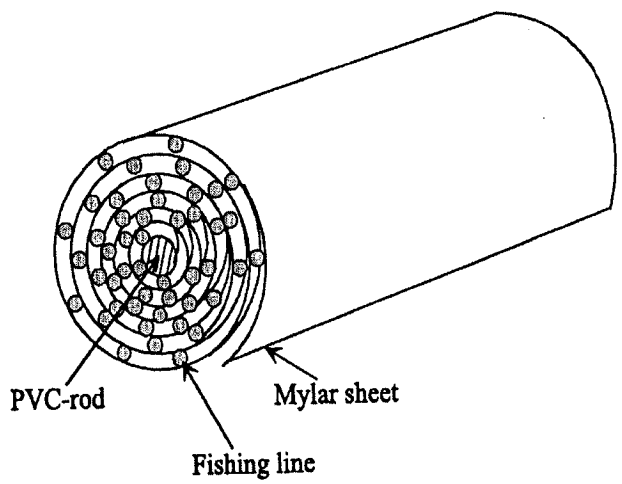

Figure 4.2: An illustration of the spiral stack [3].

4.1.4 Heat exchangers

The two heat exchangers were built from the 3/16″ diameter copper tube. To improve the performance of the heat exchangers, the tubes are bent in the form of "M"

(see Fig. 4.3). The total length of each exchanger is equal to 12 cm. The design of the heat exchangers is critical in thermoacoustics. Since they are placed in front of the stack, they block the motion of the gas particles and hence disturb the thermoacoustic process. Therefore, the heat exchangers have to be designed in a way to minimize the disturbance to the particle motion and to have the effective heat exchange between the stack and the heat exchanger fluids.

4.1.5 Assembly

A schematic illustration of the thermoacoustic refrigerator parts is shown in Fig. 4.4. It consists of an acoustic driver housing, an acoustic driver, two heat exchangers, stack, a resonator filled with air at atmospheric pressure, position adjustable piston and piston support.

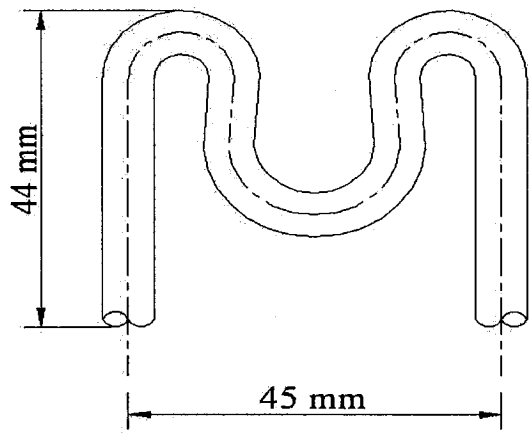

Figure 4.3: Schematic of cold and Hot Heat Exchangers

Four holes were made in the resonator tube to place heat exchangers inside the resonator tube. The first step is to place the cold heat exchanger inside the resonator. The

second step is to mount the stack and then the hot heat exchanger. Two thermocouples were attached to both sides of the stack. The inlets and outlets of both heat exchangers were extended from the resonator tube and connected with rubber pipes for the flow of water through the heat exchangers. After passing the inlet and outlet of both heat exchangers from the resonator tube wall, the holes were sealed by glue. Third step is to put the position adjustable piston into the resonator tube. Two grooves were cut on the surface of the piston where the two rubber O-rings were placed to seal the piston. The microphone was mounted in the piston to move along with the piston in the resonator as shown in Fig. 4.5. After the movable piston is mounted into the resonator tube, the support was attached to the resonator tube via six M5 bolts. Its role is to support and guide the piston. The next step is to attach the acoustic driver in its housing with the resonator tube via six M5 bolts. A groove was cut on the surface of the acoustic driver housing where a rubber O-ring was placed to seal the resonator tube. Four thermocouples were attached to the inlet and outlet of heat exchangers to measure the inlet and outlet temperatures of the circulating water through both heat exchangers.

4.2 Instrumentation

This section details the instrumentation used to collect the experimental data in the refrigerator

4.2.1 Sensors

One microphone and ten thermocouples were used in the experiments to measure the sound intensity and temperature, respectively.

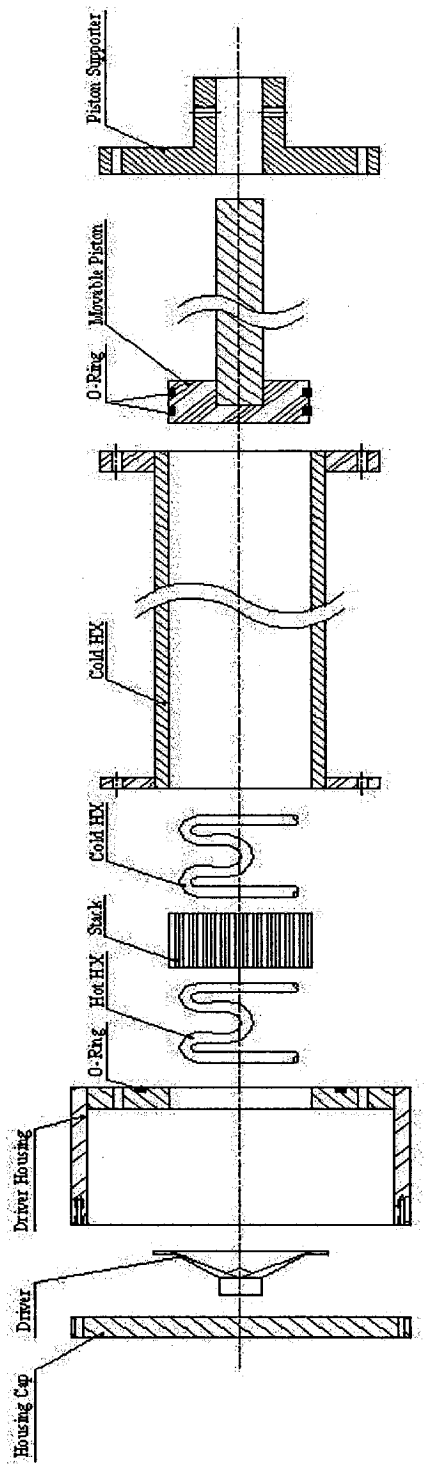

Figure 4.4: A schematic illustration of thermoacoustic refrigerator.

4.2.1.1 Microphone

A condenser microphone cartridge Model 377A10 PCB Piezotronics was used to measure the sound intensity level and dynamic pressure amplitude inside the resonator when the loudspeaker was excited. The microphone consists of a microphone cartridge and a microphone preamplifier. A preamplifier Model 426B03 was used in order to measure the sound intensity. The cartridge screws directly onto the preamplifier housing. Frequency responses are almost flat between 5Hz and 100 kHz (see Appendix A and B for the detailed specifications).

The microphone was placed in the adjustable piston as shown in Fig. 4.5. In this case microphone and piston are always at the same position i.e. at the pressure antinode, and it can always measure the maximum pressure.

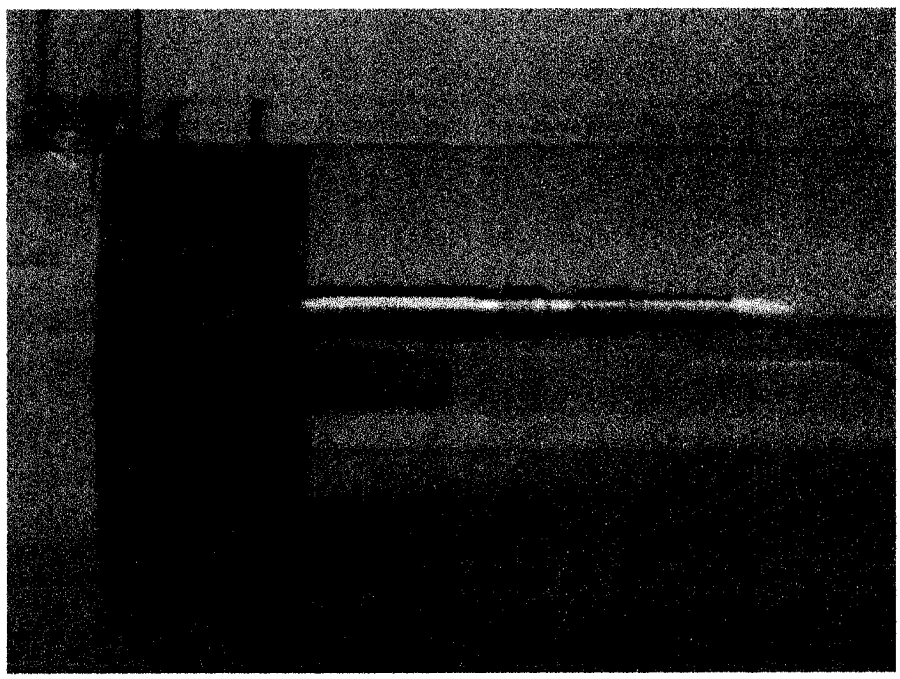

Figure 4.5: An image showing the mounted microphone in the movable piston.

4.2.1.2 Thermocouple

T-type thermocouples were used for the temperature measurements in this study. They were used to measure the temperature at different locations inside the resonator and the temperature of heat exchanger fluids. The specifications of the thermocouple are given below:

- Thermocouple Grade:-200 to 350 ^{o}C
- Limits of Error: 1.0 ^{o}C or 0.75% above 0 ^{o}C

The output of the thermocouple is very low (0.263 millivolts). A signal conditioner (SCXI-1102, National Instruments) was used to amplify and increase the signal-to-noise ratio of the original signal. The accuracy of the temperature measurement is 1 ^{o}C.

4.2.2 Electronic Devices

A Function generator model Agilent 33120A was used that could generate sine waves with different frequencies or sweep the frequency from 10 Hz to 2500 Hz, to drive the loudspeaker. An amplifier (MPA-25, Realistic) with the maximum power output of 20 watts was used to amplify the power input to the loudspeaker to increase power input. In order to acquire, process and analyze the microphone signal data, a signal analysis unit type 2035 Bruel & Kjaer and an amplifier (PCB 482A06, Piezotronics) were used.

4.2.2.1 Electronic Metering Pump

The EZ series electronic metering pump model EZB10N1-VE was used to pump water through the cold and hot heat exchangers. It consists of a pump unit, a drive unit, and a control unit. The drive unit is electromagnetic solenoid type. The specification of the pump are listed below.

Maximum Output per Stroke..... 0.11 mL
Minimum Output per Stroke..... 0.05 mL
Maximum Pressure..... 1 MP

4.2.3 Data Acquisition

A 16 channel data acquisition card (PCI-6036E, National Instruments) was used for the data acquisition. The card was installed in the PC. LabView software was used for the data acquisition. The temperature data from all thermocouples and the sound signal from the microphone were acquired simultaneously.

4.3 Measurement procedure

The Schematic of the complete electronic circuit and flow chart are shown in Fig. 4.6 and Fig. 4.7, respectively. The measured procedure is described below.

The function generator was used to generate the sine wave at 450 Hz. The wave was then amplified by the power amplifier to increase the power input to the loudspeaker.

The following measurements are made:

- Temperature (Thermocouple).
- Sound intensity (Microphone).

- Voltage and current (Loudspeaker).

The acquired data were stored on the hard drive of the PC. For each experiment two to four experimental runs were conducted to check for the consistency in the measured data. To check the accuracy of the data acquisition card, the current and voltage of the loudspeaker acquired by the card was computed with the corresponding data from the oscilloscope. The difference between the two was less than 1%. A photograph of the experimental setup instrumentation is shown in Fig. 4.8.

These types of experiments were conducted:

- Measurements inside the resonator without the stack and heat exchangers.
- Measurements inside the resonator with the stack but without the heat exchangers.
- Measurements inside the resonator with the stack and heat exchangers (i.e. the complete refrigerator)

During the third type of the experiments, the electropump was used to circulate the water through both heat exchangers. The water flow diagram is shown in Fig. 4.9 and the photograph of the setup is shown in Fig. 4.10.

In this chapter, the development of the actual components of the thermoacoustic refrigerator based on the design presented in the previous chapter, are discussed. Also, the experimental setup and experiments were described and the methods for acquiring the data and measurement were explained. The experimental results will be present in the next chapter.

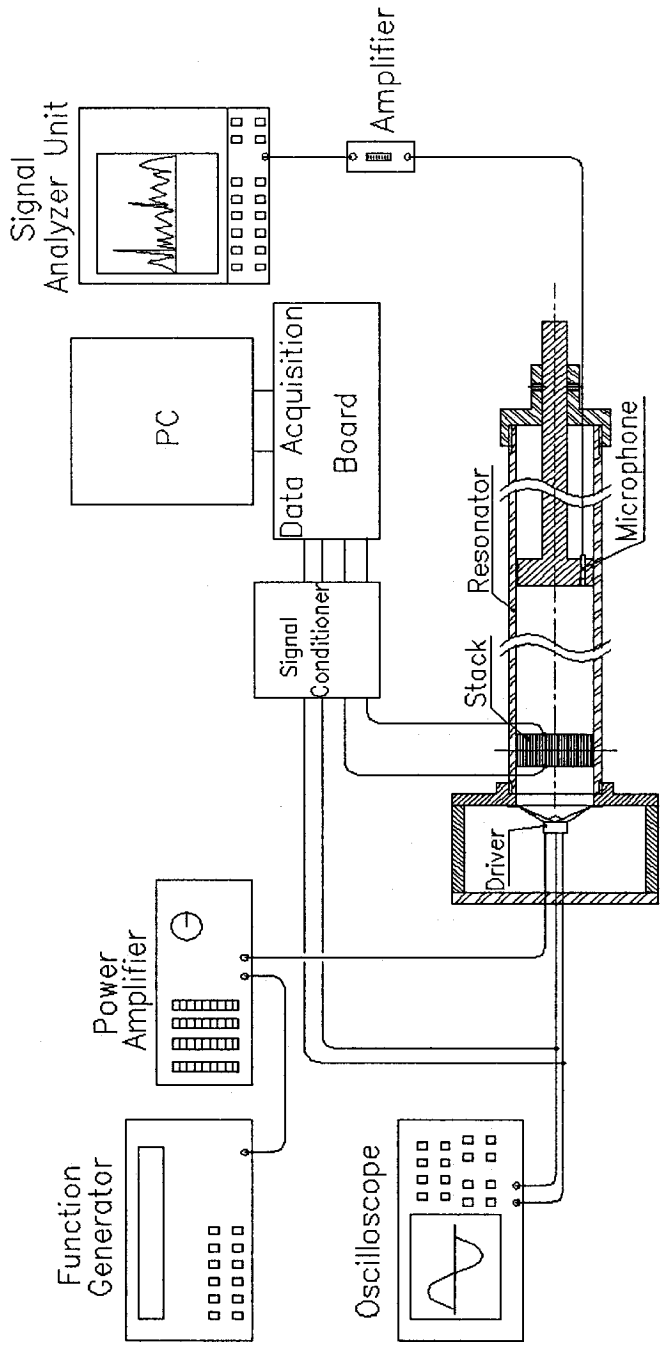

Figure 4.6: Schematic of the electric circuit diagram.

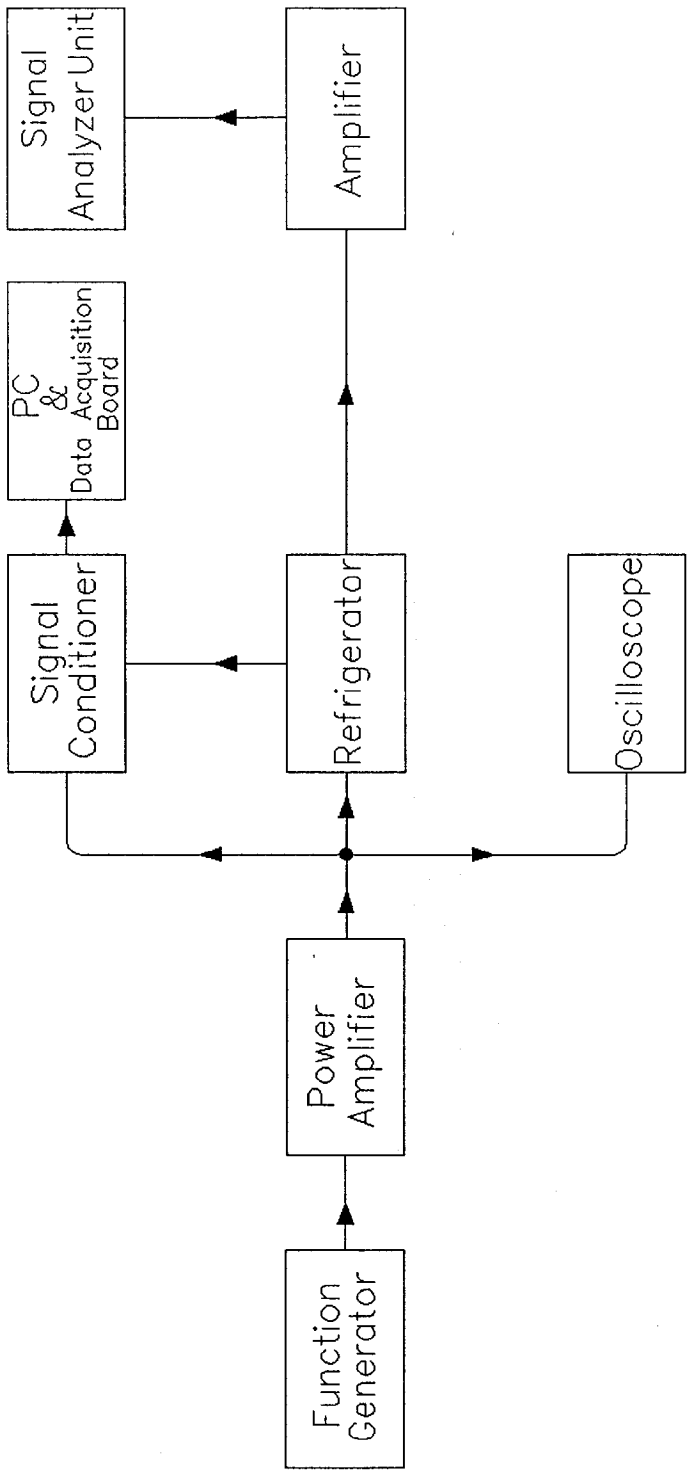

Figure 4.7: Flow diagram of experiment setting.

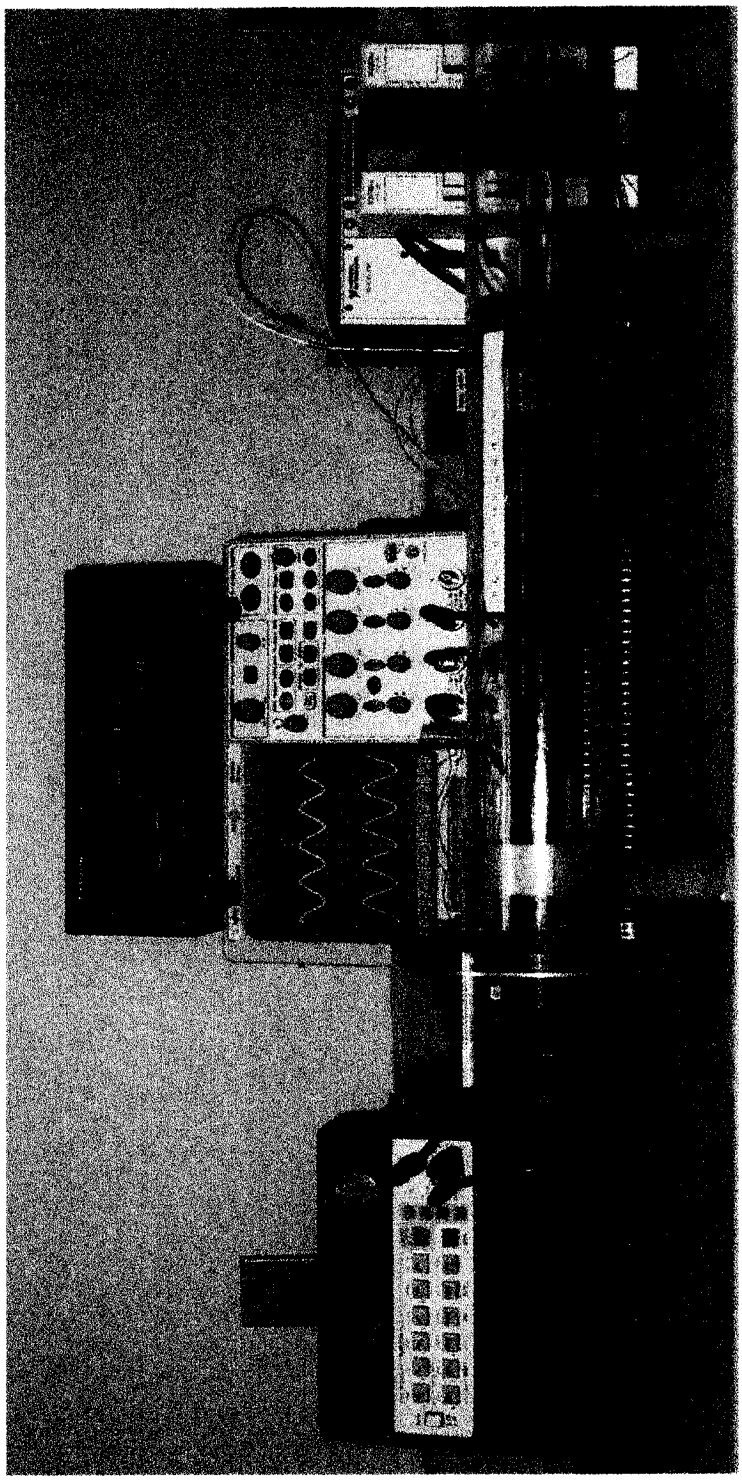

Figure 4.8: Experimental Setup for stack effect on the thermoacoustic phenomenon.

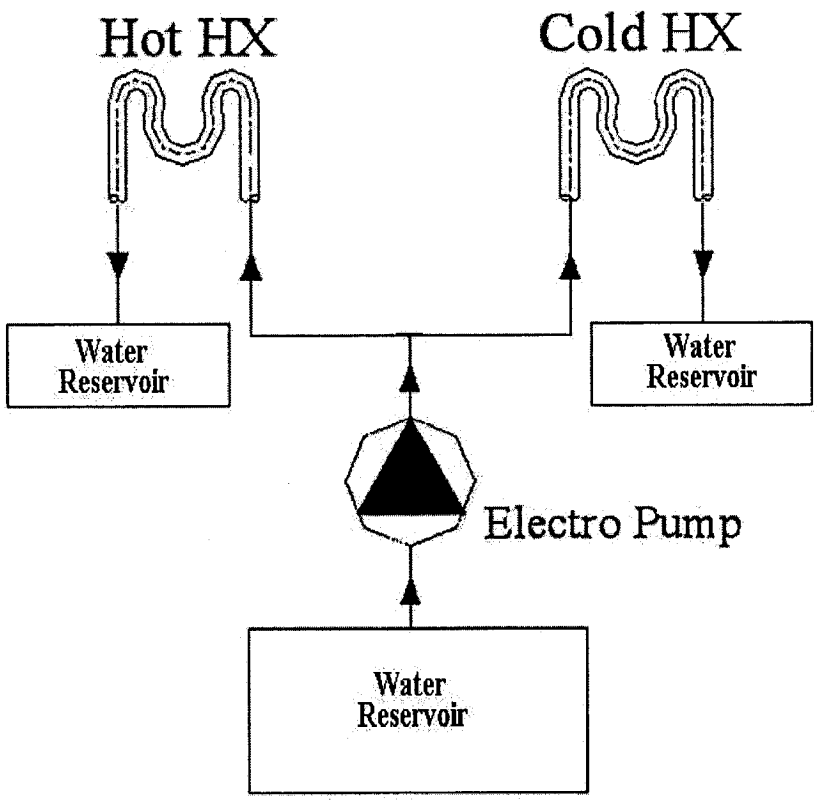

Figure 4.9: Water pumping flow diagram for both heat exchangers.

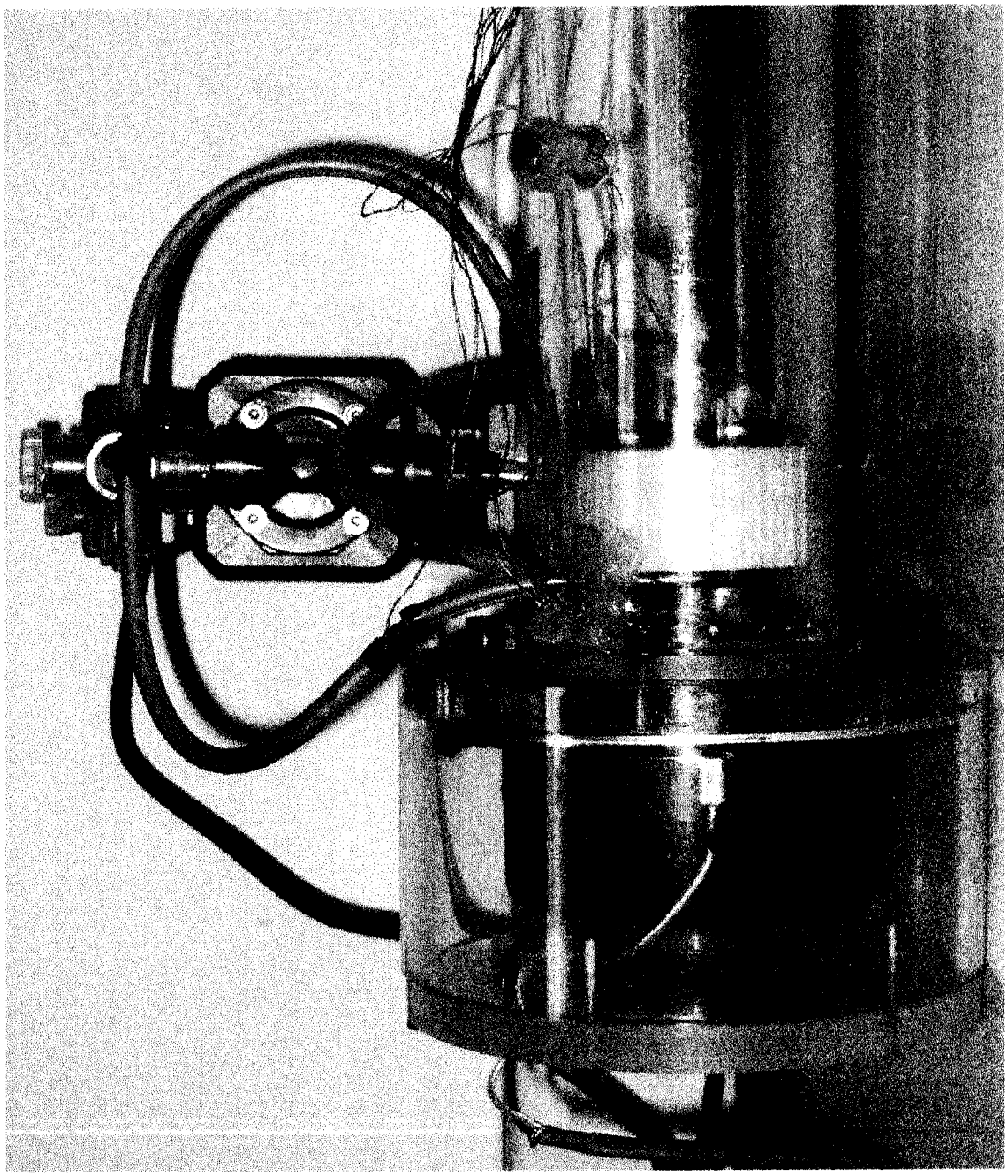

Figure 4.10: The setup for water flow in the heat exchangers.

Chapter 5

Results

In this chapter the experimental results are presented in two sections. In the first section, the results before the installation of the heat exchangers are presented and in the second section, the results of the complete system including the heat exchangers are presented.

5.1 Effect of Stack on the Thermoacoustic Phenomenon

In this section, the influence of the stack on the temperature field inside the resonator, and the effect of stack position, resonance frequency and the resonator length on the temperature difference across the stack are discussed.

5.1.1 Temperature Distribution in the Resonator Tube Without the Stack

In this set of experiments, the temperature field inside the resonator tube was measured without the stack, in the presence of the acoustic standing wave. This experiment is carried out without incorporating the stack. The temperature at 10 points inside the resonator along the length of the resonator was measured by using thermocouples. The thermocouples were placed inside the resonator 1 cm apart (see Fig. 5.1). The data was acquired for 335 seconds. The time series of the temperature field inside the resonator tube is shown in Fig. 5.2.

The figure shows that the temperature at all points remained almost constant and did not change with time. The maximum variation in the temperature along the resonator tube was 0.5 ^{o}C.

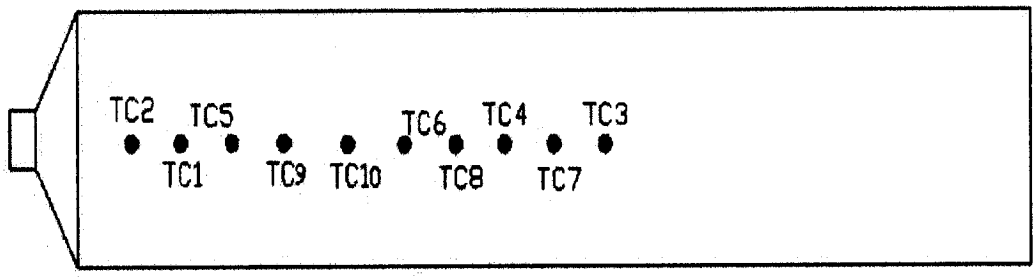

Figure 5.1: Thermocouple positions in the resonator tube without the stack.

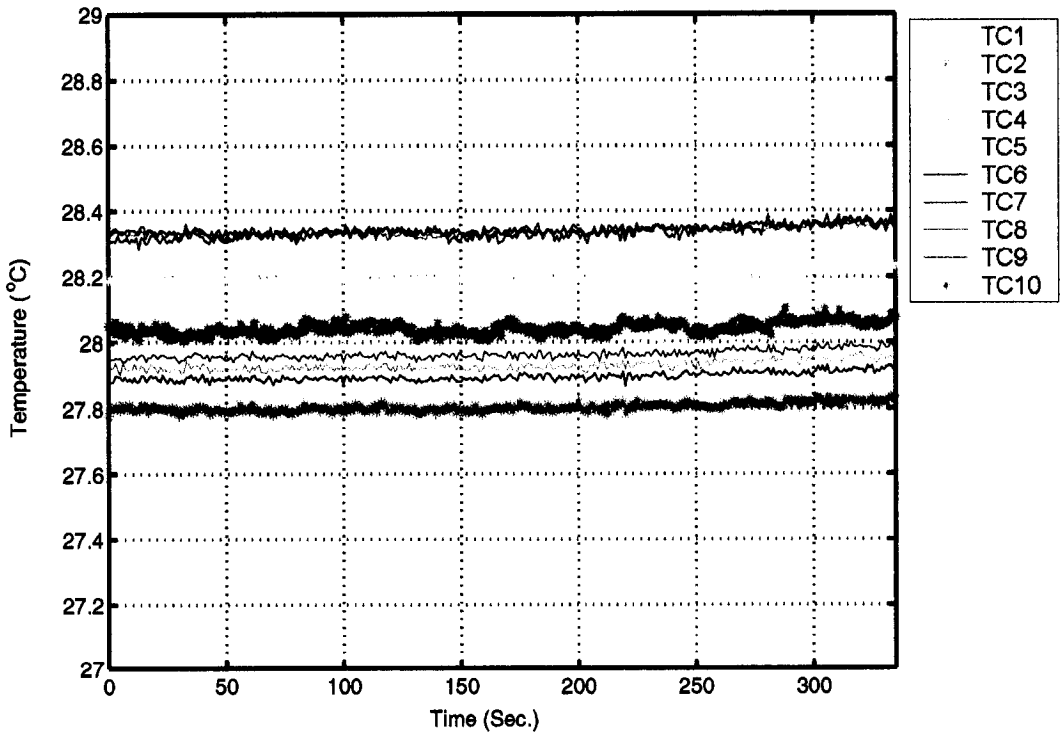

Figure 5.2: Temperature distribution at ten locations along the resonator without the stack.

5.1.2 Temperature Distribution in the Resonator Tube With Stack

In this set of experiments, the effect of the stack on the temperature field inside the resonator was investigated. The stack was mounted inside the resonator at X_s=5 cm and the acoustic standing wave was generated inside the resonator. The temperature was measured at eight points along the centerline of the resonator tube. Two thermocouples were placed on the left side of the stack, and four thermocouples were placed on right side of the stack. One thermocouple was attached to each side of the stack (see Fig. 5.3). The distance between the thermocouples was set equal to 1 cm except, the ones that were at both sides of the stack. The data was acquired for 420 seconds.

The time series of the temperature at the eight locations are plotted in Fig.5.4. The plot shows that initially all locations were at the same temperature equal to 23 ^oC. When the speaker was turned on, the standing acoustic wave was created inside the resonator, and the thermoacoustic process was initiated. Once the thermoacoustic process started, the parcels of air start transferring heat from the cold end of the stack to the hot-end. As a result, the temperature at the cold-end of the stack started to decrease and the temperature of the hot-end of the stack started to increase. The largest temperature difference was observed between the two ends of the stack. A temperature difference as high as 23 ^oC was observed across the stack approximately 400 sec after the beginning of the thermoacoustic process. It was also observed that the temperature difference decreased away from both ends of the stack.

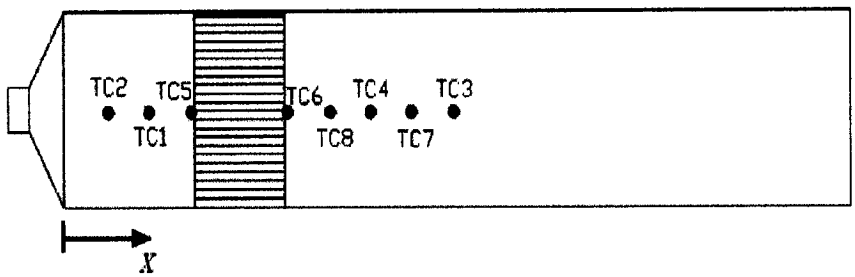

Figure 5.3: The temperature measurement positions in the resonator tube.

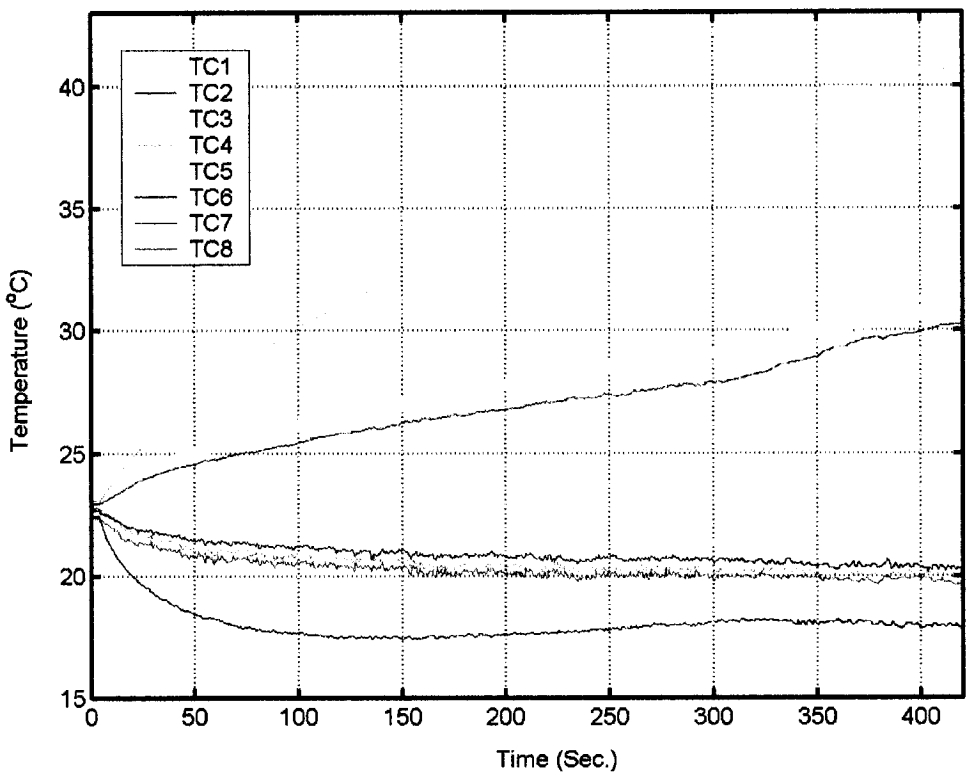

Figure 5.4: Time evolution of the measured temperature at the locations specified in Fig. 5.3.

The plot in Fig. 5.4 shows that the temperature at the hot-end of the stack increases continuously with time, whereas, the temperature at the cold-end of the stack decreases sharply during the first 110 sec, and remains constant for approximately 90 sec and then increases by 1 ^{o}C. Since this is a transient phenomenon, the analytical model, which considers the steady state phenomenon, does not predict this behavior.

The plot in Fig. 5.5 shows the temperature field inside the resonator computed from the experimental data and the numerical simulation using DeltaE software. The results show that the temperature gradient just across the stack obtained from the experiments is in good agreement with the computational results. However, the experimentally obtained temperature values in the regions on the left and right sides of the stack do not agree with the computational results. The DeltaE software predicted constant temperature in these regions. The experimental data shows that at the hot side of the resonator, as X decreases from 30 mm to 10 mm, the temperature decreases from 41 ^{o}C to 32 ^{o}C. Similarly, at the cold side of resonator, as X increases from 60 mm to 100 mm, temperature increases from 18 ^{o}C to 21.5 ^{o}C. The hot-end of the stack has the highest temperature and the cold-end of the stack has the lowest temperature inside the resonator. The main reason for this difference between theoretical and experimental results at the cold and hot side of resonator may be due to lack of good insulation. In our experiment the resonator tube is not insulated and heat is transferred between inside and outside the resonator tube.

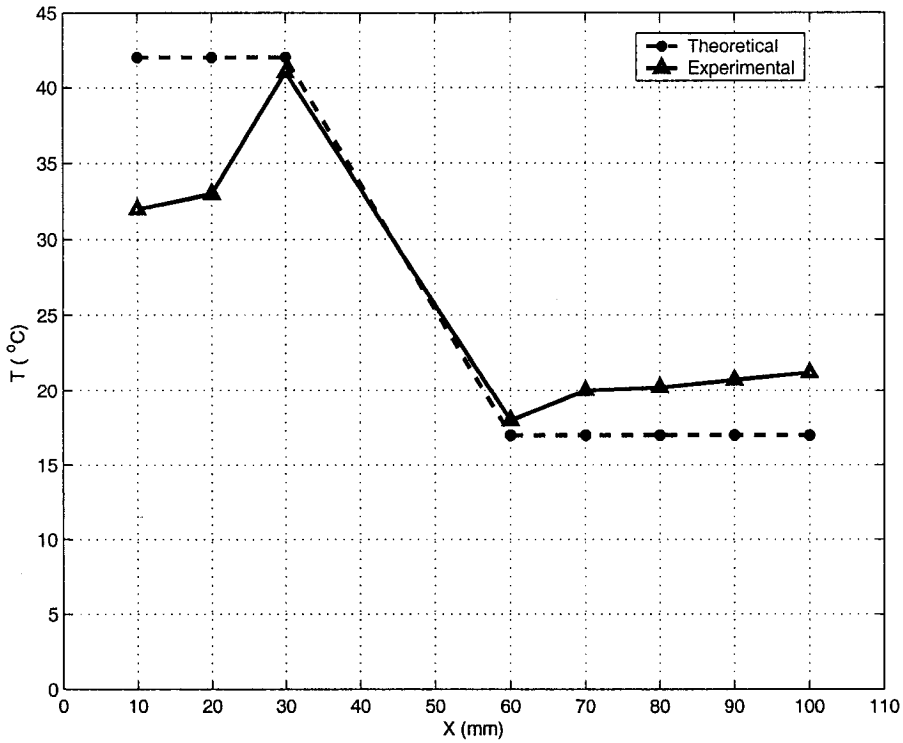

Figure 5.5: Comparison of the experimental and theoretical temperature distribution inside the resonator tube.

5.1.3 Stack Position in the Resonator Tube for Maximum Temperature Difference

The position of the stack inside the resonator is crucial for the optimum performance of the thermoacoustic refrigerator, as mentioned in section 3.4. To confirm the validity of the stack parameters obtained from the theoretical design, the position of stack (X_s) inside the resonator tube was changed from 40 mm to 190 mm (half of the resonator tube length) inside the resonator tube in 1cm increments. The power input to the speaker and operating frequency remained constant during the experiments. The temperature difference across both sides of stack was measured in each experiment for 350 sec, and the maximum temperature difference at t =350 second is tabulated in Table

5.1 and plotted in Fig. 5.6 against the stack position. The plot shows that as the stack position changed from 190 mm to 50 mm (i.e. close to a pressure antinode), the temperature difference (ΔT_m) increased from 1 ^oC to 23 ^oC. Further change in the stack position resulted in a decrease in the temperature difference. It shows that the optimum value for stack position to get maximum temperature difference is 50 mm which is in complete agreement with the theoretical study (see section 3.4.1).

Stack Position $X_s(mm)$	Temperature difference across the stack(^oC)
40	20
50	23
60	19
70	17.5
80	15
90	12.5
100	11.5
110	10
120	8.5
130	7.5
140	7
150	5
160	4
170	2.5
180	2
190	1

Table 5.1: Temperature difference across the stack, and different stack positions inside the resonator tube.

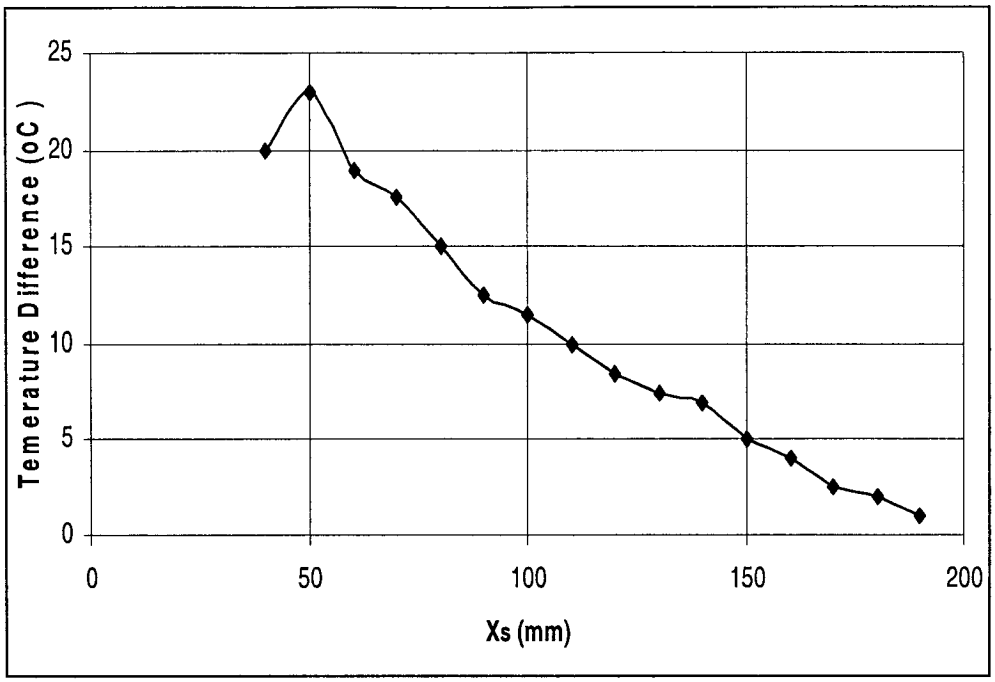

Figure 5. 6: Stack position, versus the temperature difference across the stack.

5.1.4 The Effect of the Operating Frequency on the Temperature Difference Across the Stack

The length of the resonator tube corresponds to one-half of the wavelength of the standing wave, i.e. $\lambda/2$, where λ is the wavelength of the standing wave; consequently, it is related to the operating frequency. The temperature difference across the stack was measured for different values of the operating frequency that varied from 440 Hz to 485 Hz with a 5 Hz increment. The data was acquired for 350 seconds. The stack position remained fixed at its optimal position and the power input to the speaker remained constant.

The temperature difference across the stack against operating frequency is plotted in Fig. 5.7. The plot shows that as operating frequency decreases from 485 Hz to 450 Hz,

temperature difference increases from 12 ^{o}C to 22 ^{o}C. Further decrease in frequency results in a decrease in the temperature difference. In conclusion, the optimum value of the operating frequency for this type of speaker with 385 mm length of resonator tube is 450 Hz which corresponds to half the length of the standing wave.

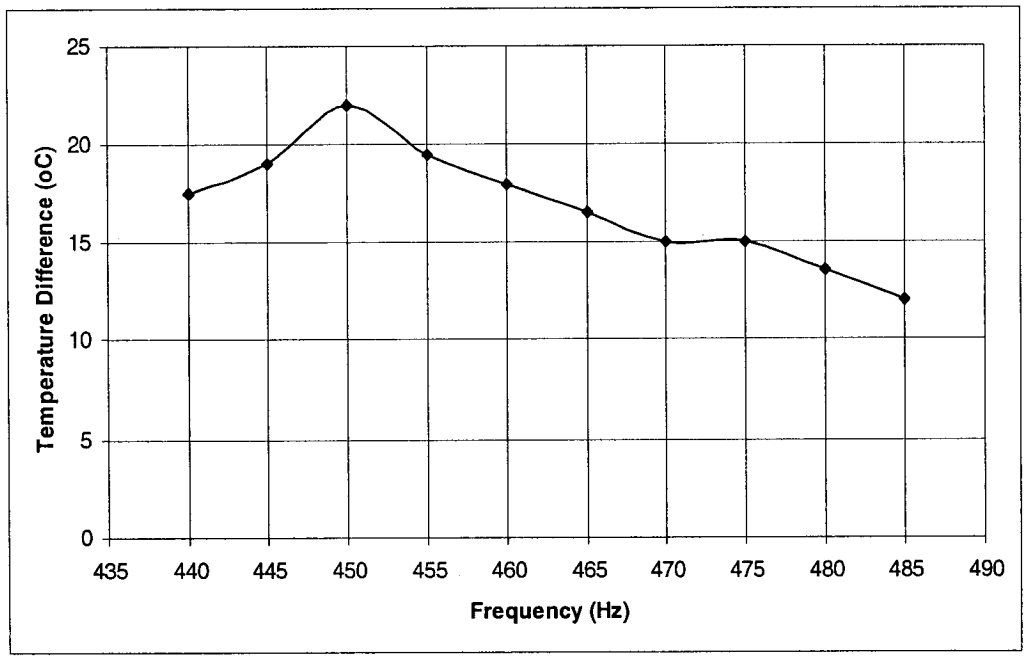

Figure 5.7: Operating frequency, versus temperature difference at both side of stack.

5.1.5 Temperature Distribution at the Stack End in the Lateral Direction

The temperature was measured in the lateral direction at the hot end of the stack at nine locations as shown in see Fig. 5.8. The time series of the temperature at nine locations are plotted in Fig. 5.9. The plot shows that initially the temperature was the same i.e. 26 ^{o}C at all points. When the speaker turned on, the temperatures started increasing at all locations. However the rate of increase in the temperature was different

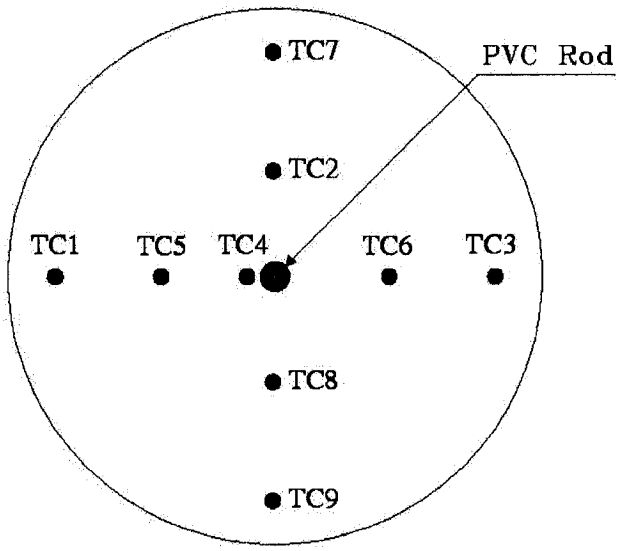

Figure 5.8: Thermocouples position on the hot side surface of stack.

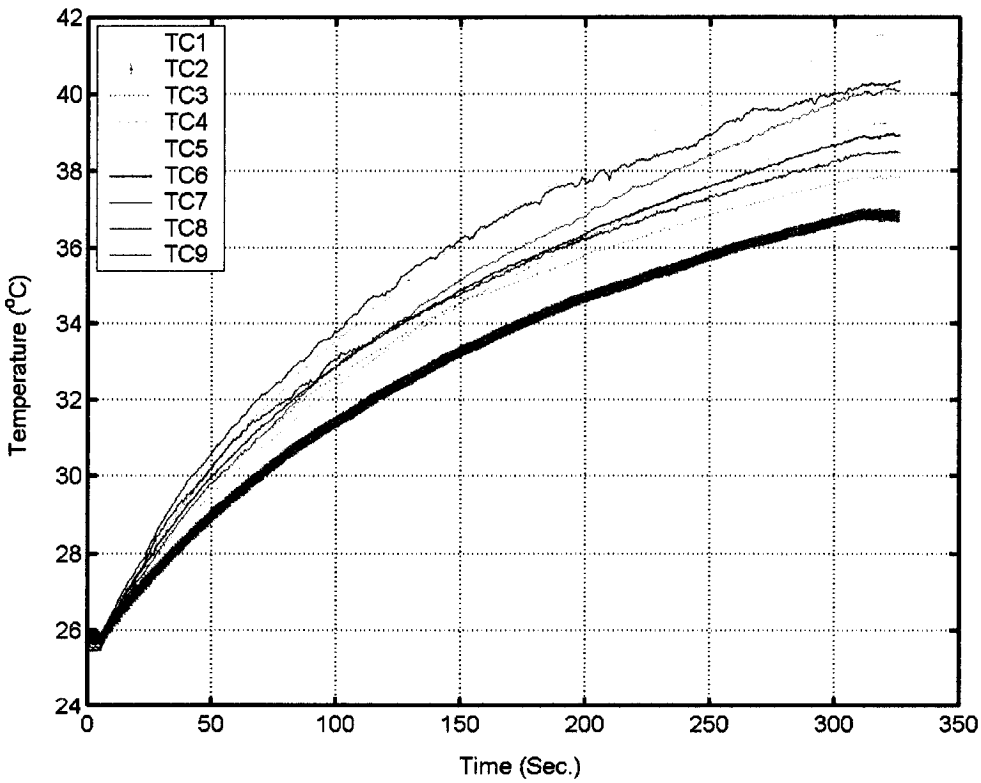

Figure 5.9: Time evolution of the temperatures at nine lateral positions at the hot end of the stack as shown in Fig. 5.8.

at different locations. The temperature was between maximum value of 41 ^{o}C, and a minimum value of 37 ^{o}C. Non homogeneous stack structure may be the cause for the difference in temperatures i.e. blockage ratio is not constant for the entire stack cross section.

5.1.6 The Effect of the Power Input on the Temperature Difference at Stack

In this set of experiments, the effect of the power input on the temperature difference across the stack was investigated. During these experiments the stack remained at its optimal position and the frequency of acoustic wave was kept at 450 Hz. The experiments were carried out at four different power inputs, ranging from 4.3 W to 12.7 W. During each experiment, the temperature was measured at both ends of the stack. The results are plotted in Fig. 5.10. The plot shows that the temperature difference across the stack is larger with higher power input.

The temperature difference at both sides of the stack at time t=190 second is plotted in Fig. 5.11 against power input to the speaker. The plot shows that as power input increased from 4.3 W to 12.7 W, the temperature difference increased from 12.5 ^{o}C to 23 ^{o}C. The plot also shows that for the power input greater than 7 W, the stack-end temperature difference increases almost linearly with the power input.

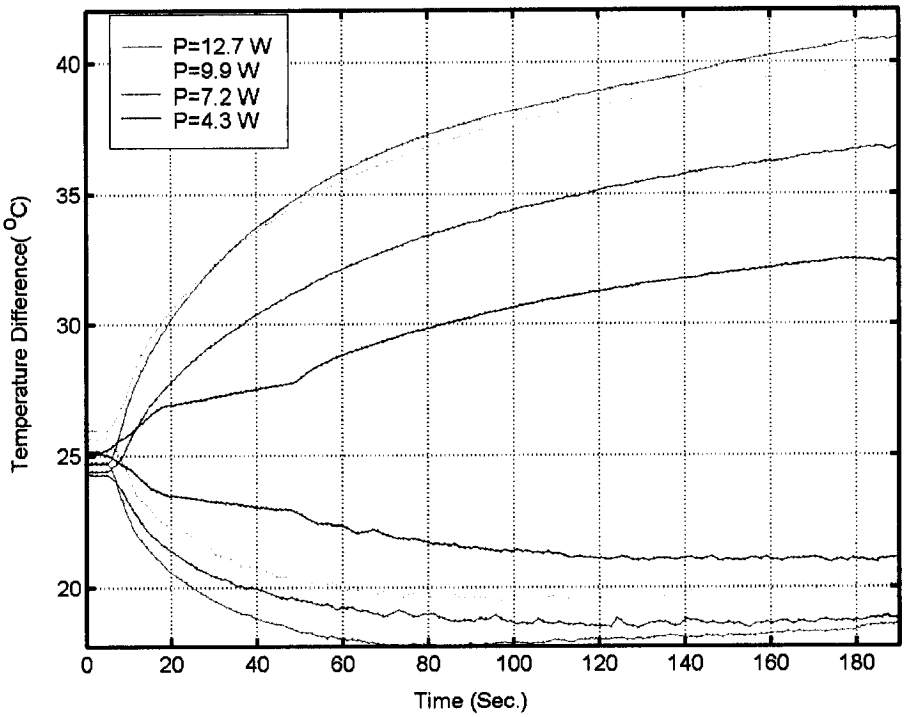

Figure 5.10: Time evolution of the measured temperature at the both ends of the stack at different power input values.

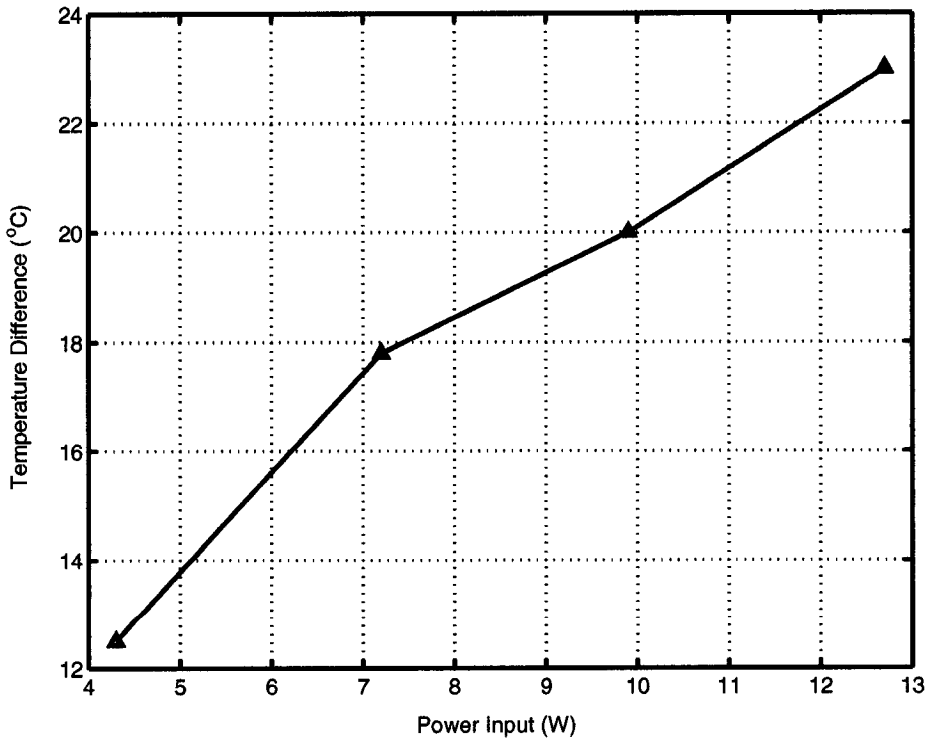

Figure 5.11: The temperature difference across the stack ends, versus the power input to the speaker.

5.2 Performance Characteristics

In the next phase of this study, heat exchangers were attached to each end of the stack and detailed measurements of temperature, pressure and sound inside the resonator were carried out. Once the heat exchangers were incorporated at both ends of the stack, the heat was extracted from the circulating fluid at the cold-end heat exchanger and, heat was added to the circulating fluid at the hot-end heat exchanger, without any significant effect on the air surrounding the stack. In this series of experiments, eight thermocouples were used to measure the temperature at both sides of the stack, water temperatures at inlet and outlet of the cold and hot heat exchangers and also at the surface of both heat exchangers (see Fig. 5.12). During these experiments the electro pump was used to circulate water through the hot and cold heat exchangers. The stack was placed at the optimum position, and the acoustic driver was driven at 450 Hz with a power input of 15.5 W.

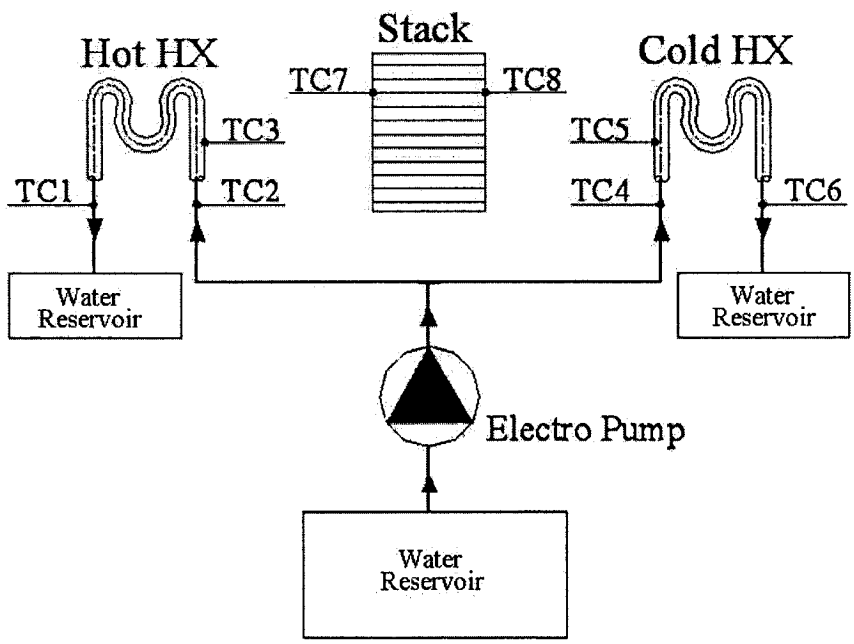

Figure 5.12: The schematic diagram showing the thermocouple positions.

5.2.1 Temperature Distribution at the Stack and the Water Temperature Difference of the Cold and Hot Heat Exchangers

Once the heat exchangers were incorporated, the refrigerator system is complete. By measuring the temperatures at the locations shown in Fig. 5.12, water flow rate through the heat exchangers, and power input to the speaker, the coefficient of performance of the refrigerator can be calculated. Fig. 5.13, Fig. 5.14, Fig. 5.15, and Fig. 5.16 show the time evolution of the measured temperature at the hot side of stack (TC7), cold side of stack (TC8), hot heat exchanger surface (TC3), Cold heat exchanger surface (TC5), inlet water to the hot heat exchanger (TC2), outlet water from the hot heat exchanger (TC1), inlet water to the cold heat exchanger (TC4), and the outlet water from the cold heat exchanger (TC6).

The plot shows that the inlet water temperature for the hot heat exchanger was almost constant at 22.5 ^{o}C, but the outlet water temperature of hot heat exchanger increased for 250 sec, and remained constant afterwards at 29 ^{o}C. Hence, the water temperature increased by 7.5 ^{o}C in the hot heat exchanger (see Fig. 5.13).

The inlet water temperature of cold heat exchanger was constant at 22.5 ^{o}C, but the outlet water temperature of cold heat exchanger decreased to 18.5 ^{o}C during the first 250 sec and for next 70 sec it increased to19 ^{o}C and remained constant afterwards. Therefore, a decrease in the water temperature by 3 ^{o}C was observed in the cold heat exchanger after 50 sec (see Fig. 5.14). However, the inlet water temperature was almost constant at 22.5 ^{o}C, and as a result, 3 ^{o}C temperature difference was established in the cold heat exchanger.

The plot shows that initially all thermocouples were at the same temperature at 22.5 ^{o}C. After 250 sec, the temperature difference across the stack reached 17 ^{o}C. The temperature at hot and cold side of the stack change sharply during the first 50 sec, but remain almost constant after 250 sec (see Fig. 5.15). The behavior of surface temperature at the cold and hot heat exchangers were very similar to the stack temperature (see Fig. 5.16).

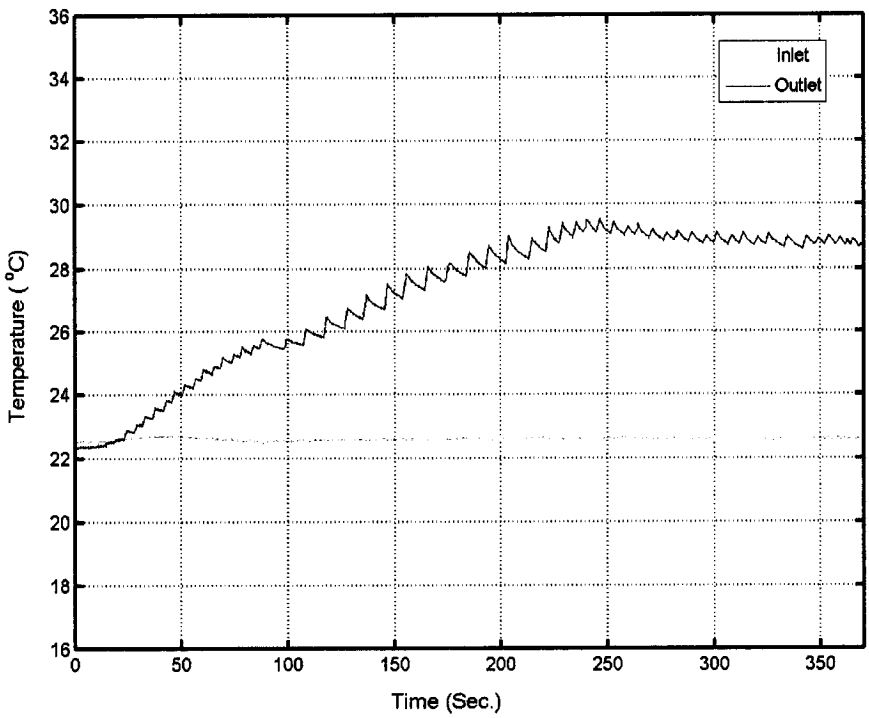

Figure 5.13: Time evolution of the measured temperatures at the water inlet and outlet of hot heat exchanger.

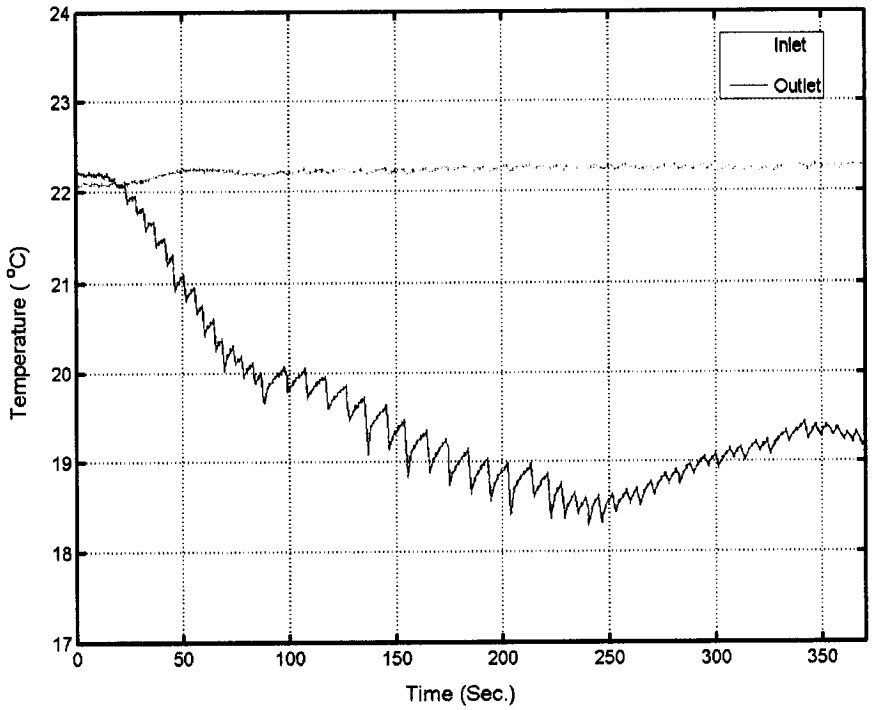

Figure 5.14: Time evolution of the measured temperatures at the water inlet and outlet of cold heat exchanger.

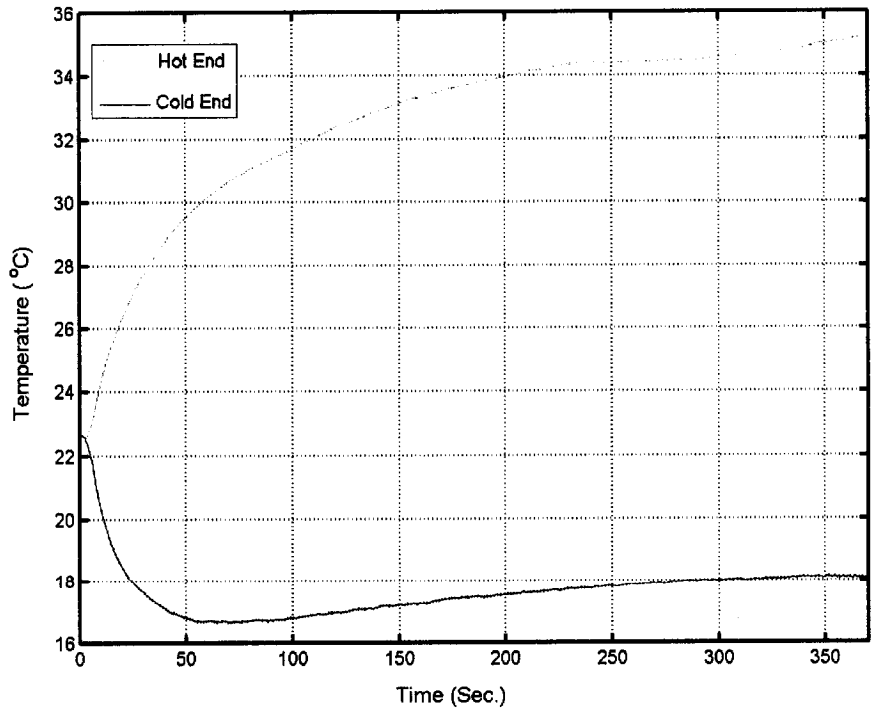

Figure 5.15: Time evolution of the measured temperatures at the ends of the central plate of the stack.

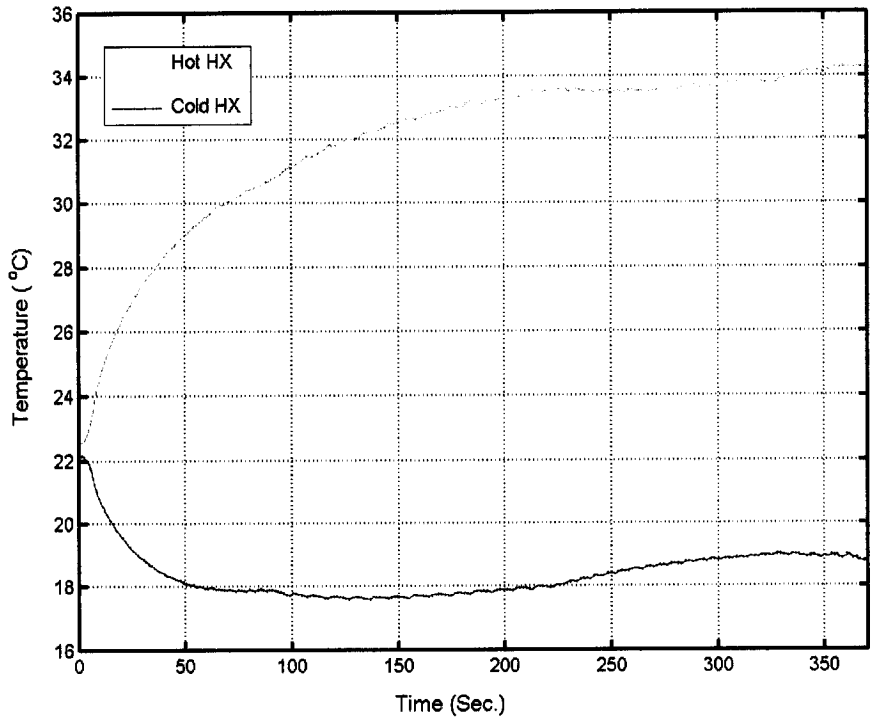

Figure 5.16: Time evolution of the measured temperatures at the heat exchangers surface.

5.2.2 The Effect of Power Input on the Heat Transfer Rate in the Cold and Hot Heat Exchangers

In this set of experiments, the effect of the power input on the heat transfer rate in both heat exchangers was investigated. The operating frequency, the stack position and the flow rates of water in both exchangers were maintained constant. The power input to the acoustic driver was changed. At each value of the power input, the temperature of water at the inlet and exit of both heat exchangers and water flow rate of both heat exchangers were recorded. The difference in the water temperatures between the inlet and outlet for cold and hot heat exchangers are plotted in Fig. 5.17 against the power input. The power input during these experiments varied from 4 W to 14.6 W. The plot shows

that as the power input increases, the temperature difference between the inlet and outlet also increases for both heat exchangers. In a heat exchanger, if the mass flow rate is constant, the temperature difference of the fluid between the inlet and outlet is proportional to the heat transfer rate. Thus, based on the given plot, it can be concluded that as the power input increases, the heat transfer rate in both heat exchangers also increases. The plot also shows that for a given power input, the heat transfer rate in the hot heat exchanger is higher than that of the cold heat exchanger. It also indicates that when the power increased from 4 W to 10 W, the heat transfer rate in both heat exchangers was low. But when the power further increased, the heat transfer rate increased relatively rapidly. The increase in the heat transfer rate in hot heat exchanger was relatively sharp.

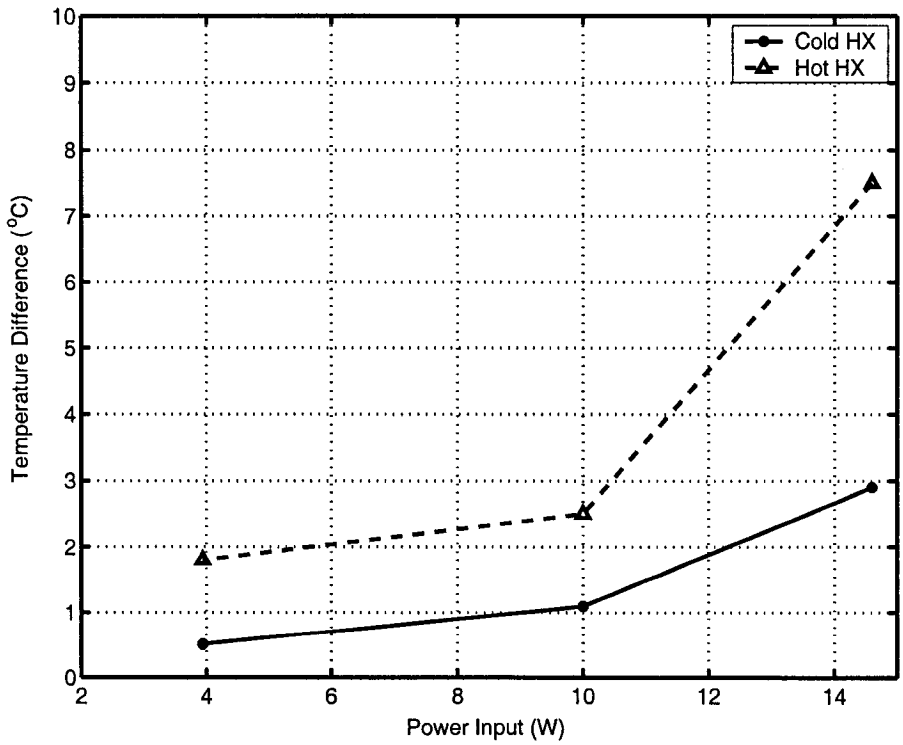

Figure 5.17: The difference of water temperature between the inlet and outlet versus the power input.

5.2.3 The Impact of Water Flow Rate on the Water Temperature Difference Across the Heat Exchangers

In this set of experiments, the operating frequency, the power input and the stack position remained constant. The flow rate of water in the hot heat exchangers was varied from 1.5 ml/min to 21 ml/min, and the flow rate of water in the cold heat exchanger was varied from 2.6 ml/min to 19.5 ml/min. The temperature difference of water between the inlet and outlet of both exchangers is plotted versus the flow rate in Fig. 5.18. The plot shows that as the flow rate increases, the difference of water temperature between the inlet and outlet decreases. At a given power input, frequency and the stack position, the heat transfer rate across the stack remains the same. In other words, the heat removal capacity at the cold-end and heat delivery capacity at the hot-end remains the same.

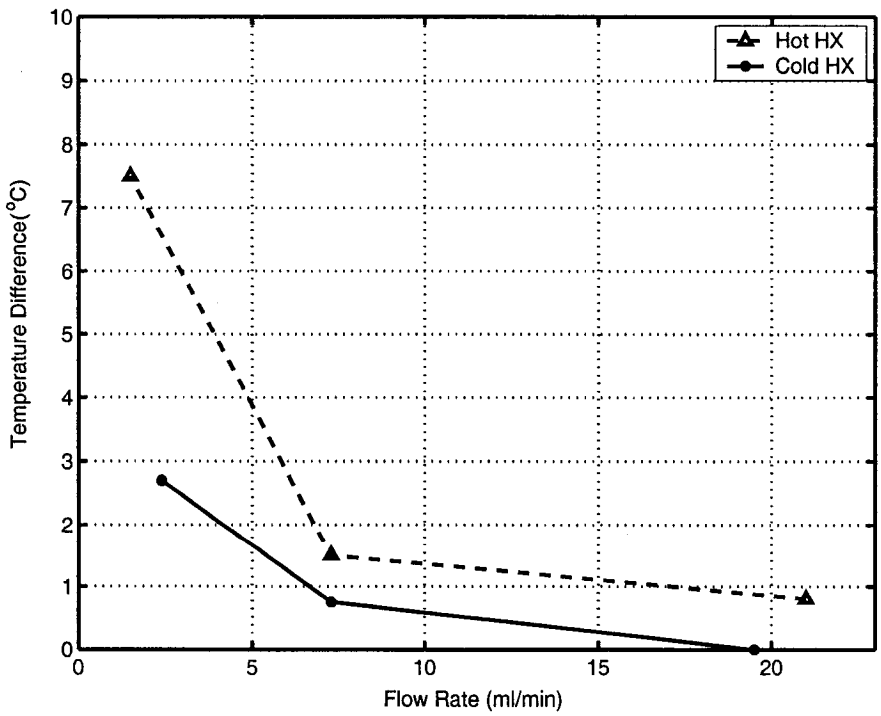

Figure 5.18: Water temperature difference at both heat exchangers, versus the electro pump flow rate.

The energy balance equation can be written as,

$$Q = \dot{m} C_p \Delta T \tag{5.1}$$

where Q is the heat transfer rate, $\dot{m}$ is the mass flow rate, C_p is the specific heat and ΔT is the fluid temperature difference between the inlet and outlet. Based on the above equation, for a constant heat transfer rate, an increase in the mass flow rate will result in a decrease in the temperature difference.

5.3 Comparison of the Experimental and Theoretical Results

The acoustic and cooling power were computed from the experimental data. For this purpose, the experiments were conducted in which the sound intensity was measured using the microphone at the pressure antinode, that is, at the right-end of the resonator, as shown in Fig. 4.5. The temperature was measured at both ends of the stack. In these experiments one microphone is used to measure the sound intensity at pressure antinode, the pressure amplitude of the acoustic wave can be estimated by applying the measured sound intensity to the Eq. (2.10). The drive ratio is ratio of the amplitude pressure to the mean pressure inside the resonator tube. It was not possible to measure the input acoustic power at the diaphragm of the loudspeaker to calculate the coefficient of performance of the thermoacoustic refrigerator.

The efficiency of the loudspeaker was used to estimate the input acoustic power for these experiments. The voltage and current at loudspeaker were measured, hence the input electrical power to the loudspeaker was computed. The acoustic power at the driver-end of the resonator can be estimated by applying the efficiency to the input

electrical power. Loudspeakers are inefficient transducers. Only about 1% of the electrical energy put into the speaker is converted to acoustic energy [32]. The remainder is converted to heat. Based on the recommendation of the loudspeaker manufacturer an efficiency of the loudspeaker was assumed to be 2%.

For numerical result, the acoustic power is calculated by using Eq.5.2;

$$W_{ac} = W_{st} + W_{res} + W_{HX} \tag{5.2}$$

where W_{st}, W_{res}, and W_{HX} are; dissipated acoustic power in stack, resonator, and heat exchangers [26]. Eq. (3.10) can be used to estimate the dissipated power in stack, and by solving the Eq. (3.3), the dissipated power can be obtained for the resonator.

By neglecting the dissipated power in the heat exchangers the acoustic power is the summation of W_{st} and W_{res}.

$$COP = \frac{Q_C}{W_{ac}} \tag{5.3}$$

The coefficient of performance against the stack temperature difference is plotted in Fig. 5.19. The figure shows that *COP* increases as temperature difference increases. It also shows that the coefficient of performance was maximum when the temperature difference was 18.6 ^oC. This value is different from the design value which is 25 ^oC. The energy dissipation increases by adding the heat exchangers, which also change the blockage ratio. Thus, the difference in the experimental and theoretical values could be due to the installation of heat exchangers.

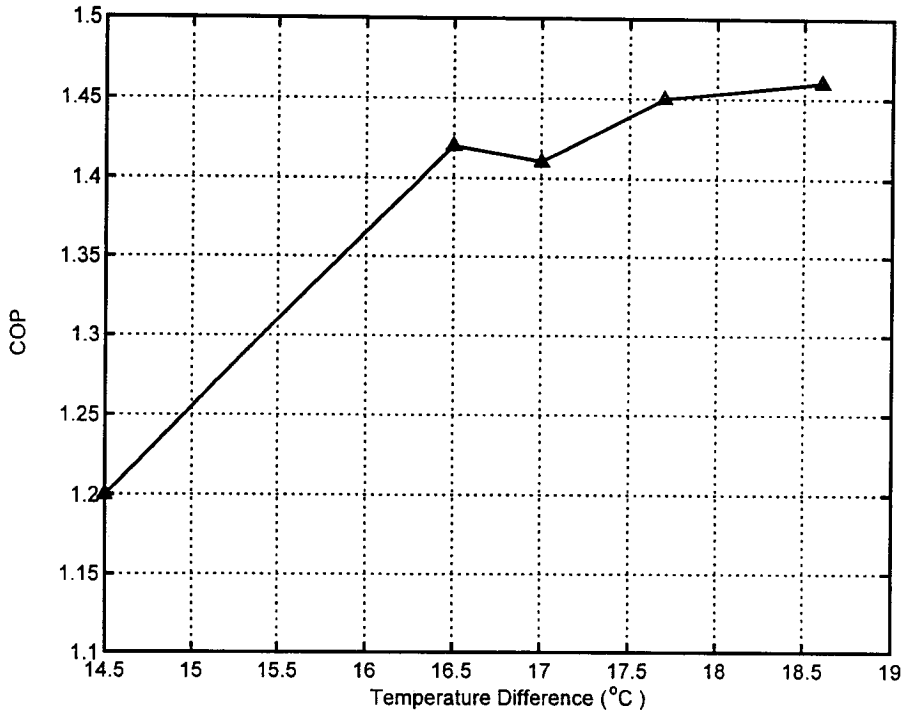

Figure 5.19: The coefficient of performance of the thermoacoustic refrigerator vs. stack temperature difference, D=0.0125, P_m=1 atm.

The COP is plotted versus Q_C in Fig. 5.20. The plot shows Coefficient of performance of the thermoacoustic refrigerator against cooling power for experimental and theoretical results. The experimental results show that COP increases from 1.2 to 1.48 as cooling power increases from 0.33 W to 0.45 W, for a given cooling power of 0.45 W, the COP obtained from the theoretical results is higher than experimental value by approximately 50%.

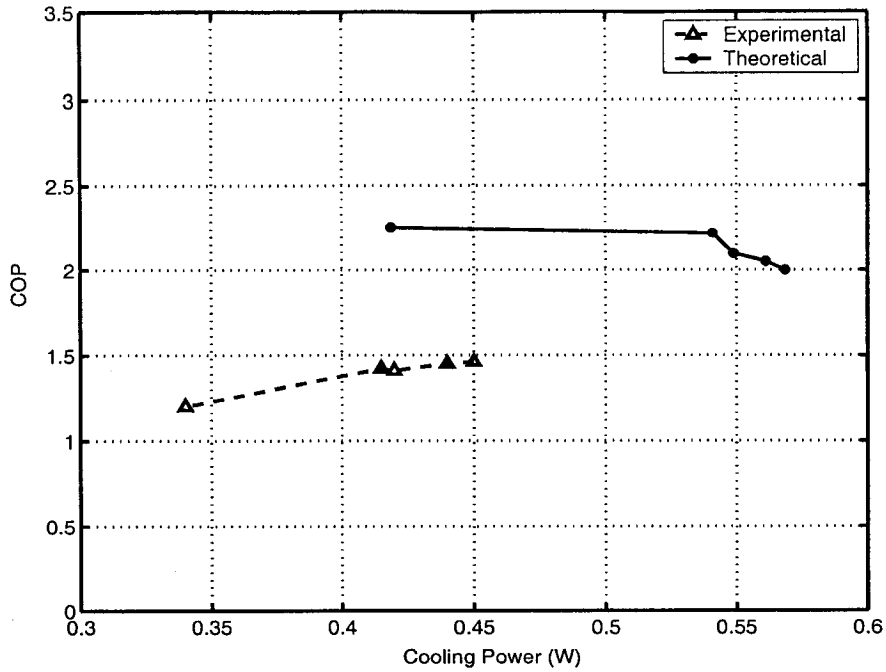

Figure 5.20: The coefficient of performance of the thermoacoustic refrigerator vs. Cooling Power, D=0.0125, P_m=1 atm.

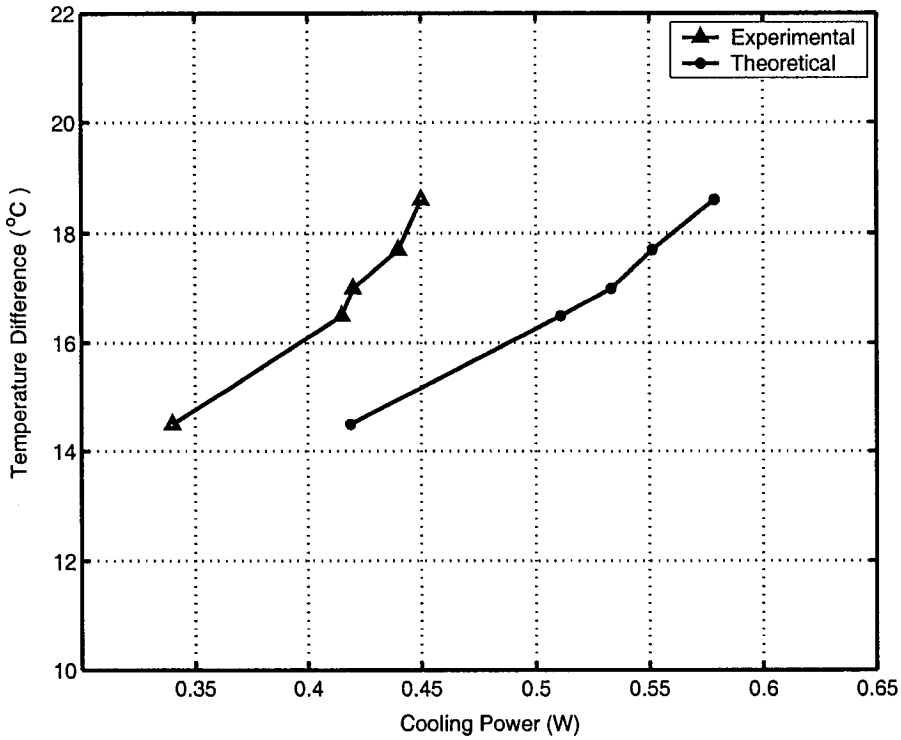

Figure 5.21: Stack temperature difference vs. cooling power, D=0.0125, P_m=1 atm.

The cooling power against the stack temperature difference is plotted for experimental and theoretical results in Fig. 5.21. The result shows that the cooling power increases as the stack temperature difference increases in the case of both experimental and theoretical results. The results also show that for a given temperature difference, the cooling power obtained from the experimental data was lower than the theoretical values. The incorporation of the heat exchangers could be the reason for this difference. The cooling power is plotted against the acoustic power for experimental and theoretical results in Fig. 5.22. Both results show that cooling power increases as acoustic power increases. However the experimental result shows that more acoustic power has been used to get cooling power compared with the theoretical results.

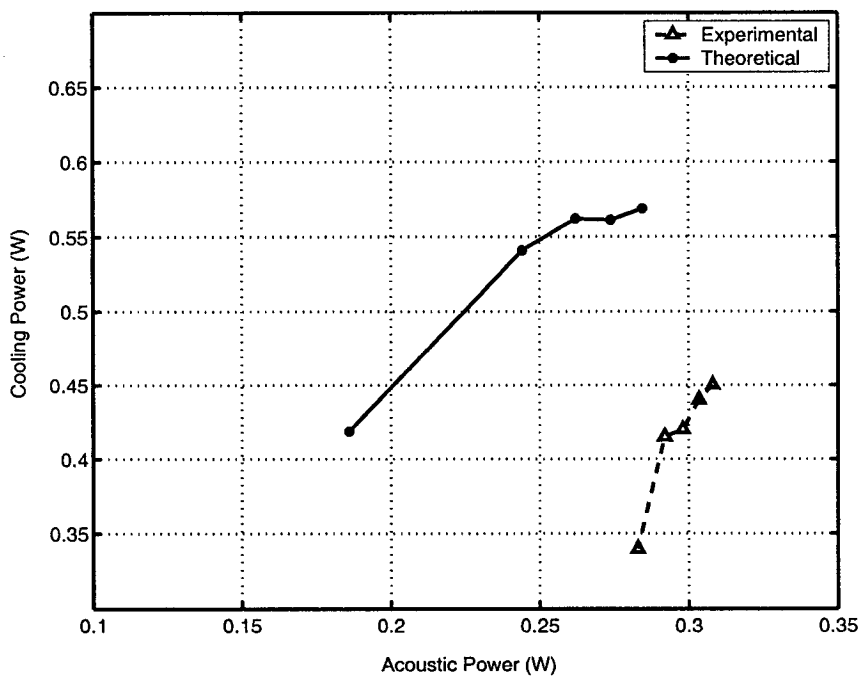

Figure 5.22: Cooling power vs. acoustic power input, D=0.0125, P_m=1 atm.

Conclusions:

The two major conclusions based on the results presented in this Chapter are:

1) There was no temperature gradient along the resonator centerline without stack. However, a temperature difference as high as 23 ^{o}C is established across the stack by adding stack inside the resonator tube.
2) Once the heat exchangers were incorporated, temperature difference as high as 7 ^{o}C at the hot heat exchanger and a temperature difference as low as 3 ^{o}C at the cold heat exchanger are established.

In this chapter the experimental results were presented for three set of experiments:

- Measurement inside the resonator without the stack and heat exchangers.
- Measurement inside the resonator with the stack but without the heat exchangers.
- Measurement inside the resonator with the stack and the heat exchangers (i.e. the complete refrigerator).

Chapter 6

Conclusions and Suggestions for the Future Work

6.1 Conclusions

Thermoacoustics is a promising area, which if properly explored, could serve as a renewable energy source. In a complete thermoacoustic system, the heat is used in the prime mover (thermoacoustic heat engine) to generate acoustic wave. This acoustic wave is then used as an input to the thermoacoustic refrigerator. Thus, a thermoacoustic system could use waste heat and drive a refrigerator. However, the efficiency of these devices is currently very low and thus, cannot compete with their conventional counterparts. The main motivation for the present work was to develop a simple thermoacoustic refrigerator that is completely functional. This thesis reports on the design and development of a simple, low-power thermoacoustic system for the refrigeration application. The design and development comprised of two parts. In the first part, which is discussed in Chapter 3, different components of the refrigerator were designed based on the given operating conditions from the theoretical analysis. The results have shown that the performance of the refrigerator depends on the working gas, pressure inside the resonator tube, shape of resonator tube, material, position and length of the stack. The performance of the stack was also simulated numerically.

In the next part, the thermoacoustic refrigerator was developed based on the design discussed in Chapter 3. The fabrication of the resonator, stack and heat exchangers, and the selection of other components are discussed in Chapter 4 along with the instrumentation and measurement procedure.

The characteristics of the fabricated refrigerator and its performance were analyzed experimentally and these experimental results are discussed in Chapter 5. The results presented in Chapter 5 are the first detailed temperature measurements inside the resonator. The results have shown that without a stack, no temperature gradient is established inside the resonator. Once the stack is placed, the temperature gradient is established across the stack. For the given operating conditions, a temperature gradient of as high as 23 ^{o}C could be established across the stack. The true performance of the refrigerator was tested after incorporating the heat exchangers on both sides of the stack. The results have demonstrated that the refrigerator extracted heat from the cold-end heat exchanger and delivered heat to the hot-end heat exchanger. The device reduced the temperature of water in the cold-end heat exchanger by 3 ^{o}C and increased the temperature of water in the hot-end heat exchanger by 7.5 ^{o}C. The cooling power of this device is estimated to be 0.45 W and the corresponding *COP* is approximately 1.5. Another merit of this device is that it could provide cooling and heating simultaneously, that is, cooling from the cold-end and heating from the hot-end.

Based on the results of the present investigations the following conclusions are drawn:

- Without the stack the temperature along the resonator tube is almost constant and the variation is within ± 0.5 °C.

- Temperature distribution along the resonator is significantly effected by the presence of the stack. After 330 sec of operation a temperature gradient of 23 ^{o}C was established across the stack.
- The position of the stack is important in order to get the maximum temperature gradient across the stack. For the resonator of 38.5 cm the position of the stack for maximum temperature gradient across the stack is 5 cm.
- The operating frequency is important in order to get the maximum temperature gradient across the stack. For the resonator of 38.5 cm the operating frequency for maximum temperature gradient is 450 Hz.
- A stack with homogenous structure is important to get the maximum temperature gradient across the stack.
- The power input is important to get the maximum temperature gradient across the stack; therefore an efficient acoustic driver is very important to get better COP.
- The cooling power of 0.45 W is provided by the device.
- The Coefficient of performance of refrigerator is approximately 1.5.

6.2 Suggestions for the Future Work

As discussed earlier, thermoacoustics is a promising technology; however, significant effort has to be done to make efficient thermoacoustic devices. The fundamental step towards the improved design is the better understanding of the gas behavior, and the temperature and pressure interactions in the device. Especially, the understanding of the gas behavior inside the stack is the key to the improvement of the

device performance. A better understanding of the gas behavior inside the stack will lead to a better design of the stack.

So far, no significant attention has been paid to the design of the heat exchanger at the two ends of the stack. Proper design of the heat exchangers is vital for the overall performance of the refrigerator, since an improper heat exchanger design could block the gas particles from entering and leaving the stack and thus, affect the device performance. Some serious attention has to be paid to the design of the heat exchangers. That is, to design heat exchangers that can minimize the blockage of the gas particles and at the same time maximize the heat exchange between the heat exchanger fluids and the stack.

The acoustic driver plays a key role in the device as it provides the input energy. The efficiencies of the common loud speakers are very low. As a result, only a fraction of the electrical energy is utilized in these devices. Some work has to be done to improve the performance of the acoustic drivers.

Based on the results of the present investigations some suggestions, for future work in order to fabricate more efficient thermoacoustic refrigerator devices are given below:

1) Fabricating and testing the refrigerator with different stack and heat exchangers types.
2) Modifying the loudspeaker in order to be used in pressurized environment.
3) Using different gases or mixture of gases as the working fluid to investigate the effect of pressure and thermodynamic properties of gases on the performance of the thermoacoustic refrigerator.

References

1) Swift G.W. "Thermoacoustic engines and refrigerators." Physics Today, 48(7): 22-28, 1995.

2) Garrett S. L., Adeff J. A., and Hofler T. J. "Thermoacoustic refrigerator for space applications." Journal of Thermoacoustics and Heat Transfer, 7(4): 595-599, 1993.

3) Tijani M.E.H., Zeegers J.C.H., and De Waele A.T.A.M. "Construction and performance of a thermoacoustic refrigerator." Cryogenics, 42(1): 59-66, 2001.

4) Bailliet H., Lotton P., Bruneau M., Gausev V., Valiere J.C., and Gazengel B. "Acoustic power flow measurement in a thermoacoustic resonator by means of laser Droppler anemometry (L.D.A) and microphonic measurement." Applied Acoustics, 60(1): 1-11, 2000.

5) Jin T., Chen G.B., Wang B.R., and Zhang S.Y. "Application of thermoacoustic effect to refrigeration." Review of Scientific Instruments, 74(1): 677-679, 2003

6) Symko O.G., Abdel-Rahman E., Kwon Y.S., Emmi M., and Behunin R. "Design and development of high-frequency thermoacoustic engines for thermal management in microelectronics." Microelectronics Journal, 35(2): 185-191, 2004.

7) Jebali F., Lubiez J. V., and Francois M. "Response of a thermoacoustic refrigerator to the variation of the driving frequency and loading." International Journal of Refrigeration, 27(2): 165-175, 2004.

8) Sakamoto S. "The experimental studies of thermoacoustic cooler." Ultrasonics, 42(1): 53-56, 2004.

9) Tijani M.E.H., Spoelstra S., Bach P.W. "Thermal-relaxation dissipation in thermoacoustic systems." Applied Acoustic, 65(1): 1-13, 2004.

10) Huelsz G., and Ramos E. "On the phase difference of the temperature and pressure waves in the thermoacoustic effect." International Communications in Heat and Mass Transfer, 22(1): 71-80, 1995.

11) Wetzel M., and Herman C. "Experimental study of thermoacoustic effects on a single plate part II: heat transfer." Heat and Mass Transfer, 35(6): 433-441, 1999.

12) Wetzel M., and Herman C. "Experimental study of thermoacoustic effects on a single plate part I: temperature fields." Heat and Mass Transfer, 36(1): 7-20, 2000.

13) Ishikawa H., and Hobson P.A. "Optimization of heat exchanger design in a thermoacoustic engine using a second law analysis." International Communications in Heat and Mass Transfer, 23(3): 325-334, 1996.

14) Ishikawa H., and David J. "Numerical investigations of flow and energy fields near a thermoacoustic couple." Journal of the Acoustical Society of America, 111(2): 831-839, 2002.

15) Waxler R. "Stationary velocity and pressure gradients in a thermoacoustic stack." Journal of the Acoustical Society of America, 109(6): 2739-2750, 2001.

16) Raspet R., Brewster J., and Bass H. E. "A new approximation method for thermoacoustic calculations." Journal of the Acoustical Society of America, 103(5): 2395, 1998.

17) Tijani M.E.H., Zeegers J.C.H., and De Waele A.T.A.M "Design of thermoacoustic refrigerators." Cryogenics, 42(1): 49-57, 2002.

18) Bensoin E., and Knio O. M. "Numerical study of thermoacoustic heat exchangers in the thin plate limit." Numerical Heat Transfer-Part A-Applications, 40(5): 455-471, 2001.

19) Biwa T., Sunahara S., and Mitzutani U. "Thermoacoustic effect in a Gifford-Mcmahon refrigerator." Journal of Applied Physics, 92(10): 6334-6336, 2002.

20) Ried R.S., and Swift G.W. "Experiments with a flow-through thermoacoustic refrigerator." Journal of the Acoustical Society of America, 108(6): 2835-2842, 2000.

21) Herman C., and Wetzel M. "Design optimization of thermoacoustic refrigerators." International Journal of Refrigeration, 20(1): 3-21, 1997.

22) Piccolo A., and Cannistraro G. "Convective heat transport along a thermoacoustic couple in the transient regime." International Journal of Thermal Science, 41: 1067-1075, 2002.

23) Tijani E.H., Zeeger J.C.H., and De waele A.T.A.M. "The optimal stack for thermoacoustic refrigeration." Journal of the Acoustical Society of America, 112(1): 128-133, 2002.

24) "Major appliance industry in Canada, Industry Canada." Internet: http://www.strategis.gc.ca/

25) Cengel Y. A., and Boles M. "Thermodynamics: An Engineering Approach." Fourth Edition, McGraw-Hill, New York, 2001.

26) Tijani E.H. "Loudspeaker-driven thermo-acoustic refrigeration." Ph.D. thesis, Technische Universeit Eindhoven, The Netherlands, 2001.

27) Swift G. W. "Thermoacoustics: a unifying perspective for some engines and refrigerators." available from the Acoustical Society of America, 1999.

28) Everest F. "Master handbook of acoustics." Fourth Edition, McGraw-Hill, New York, 2001.

29) Andersson P. B. U., and Kropp W. "Review of thermoacoustic refrigeration." Master thesis, Chalmers University of Technology, Sweden, 1999.

30) Rizonni G. "Principles and applications of electrical engineering." Third Edition, McGraw-Hill, New York, 2000.

31) Ward B., and Swift G. W. "Design environment for low-amplitude thermoacoustic engines DELTAE version 1.1 tutorial and user's guide." Internet: http://www.lanl.gov/projects/thermoacoustics/Manual/DelEdoc.html

32) "Dynamic loudspeakers." Internet: http://www.wordiq.com/definition/Loudspeaker#Efficiency

APPENDIX A

PERFORMANCE	
Response	Pressure
Open Circuit Sensitivity (at 250 Hz)	1.6 mV/Pa
Frequency Response (±2 dB)	4 Hz to 70 kHz
Polarization Voltage	0 V [1]
Dynamic Range - 3% Distortion Limit	170 dB
Dynamic Range - Cartridge Thermal Noise	34 dB (A)
ENVIRONMENTAL	
Temperature Range (Operating)	-40 to 150 °C
Temperature Response	<0.03 dB
Humidity Range (Non-Condensing)	0 to 95 %RH
Humidity Sensitivity	<0.03 dB
ELECTRICAL	
Excitation Voltage	20 to 32 VDC
Constant Current Excitation	2 to 20 mA
Impedance (Input)	$<2x10^{10}$ ohms
Capacitance (Input)	0.15 pF
Output Bias Voltage	10 to 14 VDC
Impedance (Output)	<50 ohms
Output Voltage (Maximum)	>8 Vpk
PHYSICAL	
Diameter	1/4"
Weight	2 g (0.07 oz)

Microphone Specifications

APPENDIX B

PERFORMANCE	
Nominal Microphone Diameter	1/4"
Gain	-0.15 dB
Frequency Response (± 0.1 dB)	5 to 100,000 Hz
(-3 dB)	<1 Hz
Phase Linearity (<1 °)	63 to 20,000 Hz
Electrical Noise (A-weight)	<3.2 μV
(Flat 20 Hz to 20 kHz)	<5.6 μV
Distortion (3 Vrms input at 1KHz)	<-70 dB
Output Slew Rate	2 V/μS
TEDS Compliant	Yes
ENVIRONMENTAL	
Temperature Range (Operating)	-40 to 158 °F
Temperature Response	<0.03 dB
Humidity Range (Non-Condensing)	0 to 95 %RH
Humidity Sensitivity	<0.03 dB
ELECTRICAL	
Excitation Voltage	20 to 32 VDC
Constant Current Excitation	2 to 20 mA
Impedance (Input)	$<2x10^{10}$ ohms
Capacitance (Input)	0.15 pF
Output Bias Voltage	10 to 14 VDC
Impedance (Output)	<50 ohms
Output Voltage (Maximum)	>8 Vpk
PHYSICAL	
Size (Diameter x Length)	0.25 in x 1.74 in
Weight	0.21 oz

Preamplifier Specifications

APPENDIX C

Frequency Characteristics
Sine ..... 100 μHz - 15 MHz
Resolution ..... 10 μHz or 10 digits
Accuracy ..... 20 ppm in 1 year
Temp. Coeff (18°C - 28°C) < 2 ppm/°C
Output Characteristics
Amplitude (into 50_) ..... 50 mVpp - 10 Vpp
Accuracy (at 1 kHz)..... ± 1% of specified output
Flatness (sinewave relative to 1 kHz) ... < 100 kHz ± 1% (0.1 dB)
Output Impedance .....50Ω (fixed)
Sweep
Type..... Linear or Logarithmic
Direction..... Up or Down
Start F/Stop F ..... 10 mHz - 15 MHz
Speed ..... 1 ms to 500 s ± 0.1%
Trigger..... Single, External, or Internal

Function Generator Specifications

APPENDIX D

Normal Range at Full (V)	Absolute Accuracy							Relative Accuracy	
	% of Reading		Offset	Notee+Quantization (uV)		Temp Drift(%/°C)	Absolute Accuracy at Full Scale (mV)	Resolution (uV)	
	24 Hour	lYear	(UV)	Single PL	Averaged			Single	Averaged
±10	0.054	0.0588	±160	±933	±82.4	0.0010	7.56	1,085	108.5
±5	0.014	0.0188	±811	±467	±41.2	0.0005	1.79	542	52.24
±0.5	0.054	0.0588	±100	±56.2	±5.04	0.0010	0.399	66.3	6.630
±0.05	0.0546	0.0588	±28.9	±28.2	±2.75	0.0010	0.0611	36.2	3.616

Input accuracy information of data acquisition board NI 6036E

Nominal Range at Full Scale (V)	Absolute Accuracy					
	% of Reading			Offset (mV)	Temp Drift (%/°C)	Absolute Accuracy at Full Scale (mV)
	24 Hours	90 Days	lYear			
±10	0.0089	0.0109	0.0131	±0.103	0.0005	2.41

Output accuracy information of data accusation board NI 6036E

Analog Input Characteristics

Number of channels .....16 single-ended or 8 differential(software-

selectable per channel)Resolution .....16 bits, 1 in 65,536

Sampling rate .....200 kS/s guaranteed

Input signal ranges .....Bipolar only

Input coupling .....DC

Maximum working voltage(signal + common mode) ..... Each input should remain within ±11 V of ground

Analog Output Characteristics

Number of channels.....2 voltage

Resolution.....16 bits, 1 in 65,536

Voltage Output
Range .....±10 V
Output coupling .....DC
Output impedance.....0.1Ω max
Current drive.....±5 mA max
Protection.....Short-circuit to ground
Dynamic Characteristics
Settling time for full-scale step.....10 µs to ±4 LSB accuracy
Slew rate.....15 V/µs
Noise.....110 µVrms, DC to 400 kHz
Midscale transition glitch
Magnitude..... ±10 mV
Duration..... 1.0 µs
Stability
Offset temperature coefficient..... ±35 µV/°C
Gain temperature coefficient..... ±6.5 ppm/°C
Digital I/O
Number of channels.....8 input/output
Compatibility.....TTL/CMOS